© 2018. Published by The Company of Biologists Ltd | Development (2018) 145, dev158782. doi:10.1242/dev.158782

RESEARCH ARTICLE

Nesprins and opposing microtubule motors generate a point force that drives directional nuclear motion in migrating neurons

You Kure Wu[1], Hiroki Umeshima[2,*], Junko Kurisu[2] and Mineko Kengaku[1,2,*]

ABSTRACT

Nuclear migration of newly born neurons is essential for cortex formation in the brain. The nucleus is translocated by actin and microtubules, yet the actual force generated by the interplay of these cytoskeletons remains elusive. High-resolution time-lapse observation of migrating murine cerebellar granule cells revealed that the nucleus actively rotates along the direction of its translocation, independently of centrosome motion. Pharmacological and molecular perturbation indicated that spin torque is primarily generated by microtubule motors through the LINC complex in the absence of actomyosin contractility. In contrast to the prevailing view that microtubules are uniformly oriented around the nucleus, we observed that the perinuclear microtubule arrays are of mixed polarity and both cytoplasmic dynein complex and kinesin-1 are required for nuclear rotation. Kinesin-1 can exert a point force on the nuclear envelope via association with nesprins, and loss of kinesin-1 causes failure in neuronal migration *in vivo*. Thus, microtubules steer the nucleus and drive its rotation and translocation via a dynamic, focal interaction of nesprins with kinesin-1 and dynein, and this is necessary for neuronal migration during brain development.

KEY WORDS: Neuronal migration, Cerebellum, Nucleus, Nesprin, Microtubules, Kinesin-1, Mouse

INTRODUCTION

During mammalian brain development, newly born neurons migrate from their birthplace in the germinal layers to their final destination in the emerging cortices and nuclei, where they are eventually integrated into functional neural circuits. Migration of postmitotic neurons is an essential step in brain development, and its failure is associated with various brain disorders (Manzini and Walsh, 2011; Cooper, 2013; Moon and Wynshaw-Boris, 2013). Migrating neurons typically exhibit a bipolar shape with a long, thick leading process extending from the cell soma toward its destination, followed by a thin trailing process on the opposite site of the soma. The nucleus in the cell soma is translocated into the preceding leading process through the crowded neural tissue by the force generated by actin, microtubules and related motor proteins (Vallee et al., 2009; Trivedi and Solecki, 2011). The actomyosin contractile force plays a major role in driving nuclear translocation, exerting either a pulling force in the leading process or a pushing force in the cell rear (Bellion et al., 2005; Schaar and McConnell, 2005; Solecki et al., 2009; He et al., 2010; Martini and Valdeolmillos, 2010; Shinohara et al., 2012). Perinuclear microtubules emanating from the leading process and their associated cytoplasmic dynein complex are also indispensable for directional motion of the nucleus (Shu et al., 2004; Tanaka et al., 2004; Tsai et al., 2007; Umeshima et al., 2007). These cytoskeletons and associated motors are anchored to the protein complexes embedded in the nuclear membrane, including the linker of nucleoskeleton and cytoskeleton (LINC) complex and the nucleopore complex, by which they transduce the force to the nucleus (Crisp et al., 2006; Zhang et al., 2009; Hu et al., 2013). However, the precise interplay of actomyosin and microtubules during nuclear translocation as well as the site and extent of the force generated by these cytoskeletons remain to be elucidated.

Here, we observed the dynamic motion of the nucleus in migrating cerebellar granule cells (CGCs) at a high spatiotemporal resolution using spinning-disk confocal microscopy, in order to enhance our understanding of the mechanism and dynamics of nuclear migration in neurons. We found that the nucleus in migrating neurons displays a highly dynamic motion, including fast rotation in the soma along the direction of its translocation. We demonstrate that the nuclear rotation and some mode of nuclear translocation are driven by the motor activity of cytoplasmic dynein complex and kinesin-1, which is transmitted to the nucleus via the LINC complex. By contrast, actomyosin appeared not to be involved in nuclear rotation, suggesting that actin and microtubules act somewhat independently and control different modes of nuclear dynamics during neuronal migration.

RESULTS

The nucleus frequently rotates during neuronal migration

Tangential migration of the CGCs can be reconstituted in a reaggregate culture (Umeshima et al., 2007). At 1-2 days *in vitro* (DIV), each CGC extended a long leading process and migrated out of the cell aggregate at an average somal speed of 12.2±1.5 µm/h. In differential interference contrast time-lapse imaging, we observed that the nucleus sometimes rotated during migration, as determined by the relative position of the nucleoli (Fig. S1A). The nucleoli appeared to rotate more than 30° in 1 min. To perform more detailed image analysis, we labeled heterochromatin as a position marker in the nucleus by transfecting heterochromatin protein 1 beta (HP1β)-mCherry (HP1β is also known as Cbx1) together with a GFP cell-volume marker (Dialynas et al., 2006). Consistent with previous reports, heterochromatin formed focal aggregates in the nucleoplasm and nuclear periphery in the CGCs. Time-lapse imaging with spinning-disk confocal microscopy at 15 s intervals revealed that the nucleus is highly dynamic during neuronal migration, exhibiting frequent deformation from a round to an irregular oval shape (Movie 1, left). In addition, the heterochromatin spots exhibited intermittent rotation in the cell soma of highly

[1]Graduate School of Biostudies, Kyoto University, Yoshida Honmachi, Sakyo-ku, Kyoto 606-8501, Japan. [2]Institute for Integrated Cell-Material Sciences (WPI-iCeMS), Kyoto University, Yoshida Honmachi, Sakyo-ku, Kyoto 606-8501, Japan.

*Authors for correspondence (umeshima@icems.kyoto-u.ac.jp; kengaku@icems.kyoto-u.ac.jp)

H.U., 0000-0001-9957-1468; M.K., 0000-0002-1666-3648

Received 23 August 2017; Accepted 29 January 2018

Development (2018) 145, dev158782. doi:10.1242/dev.158782

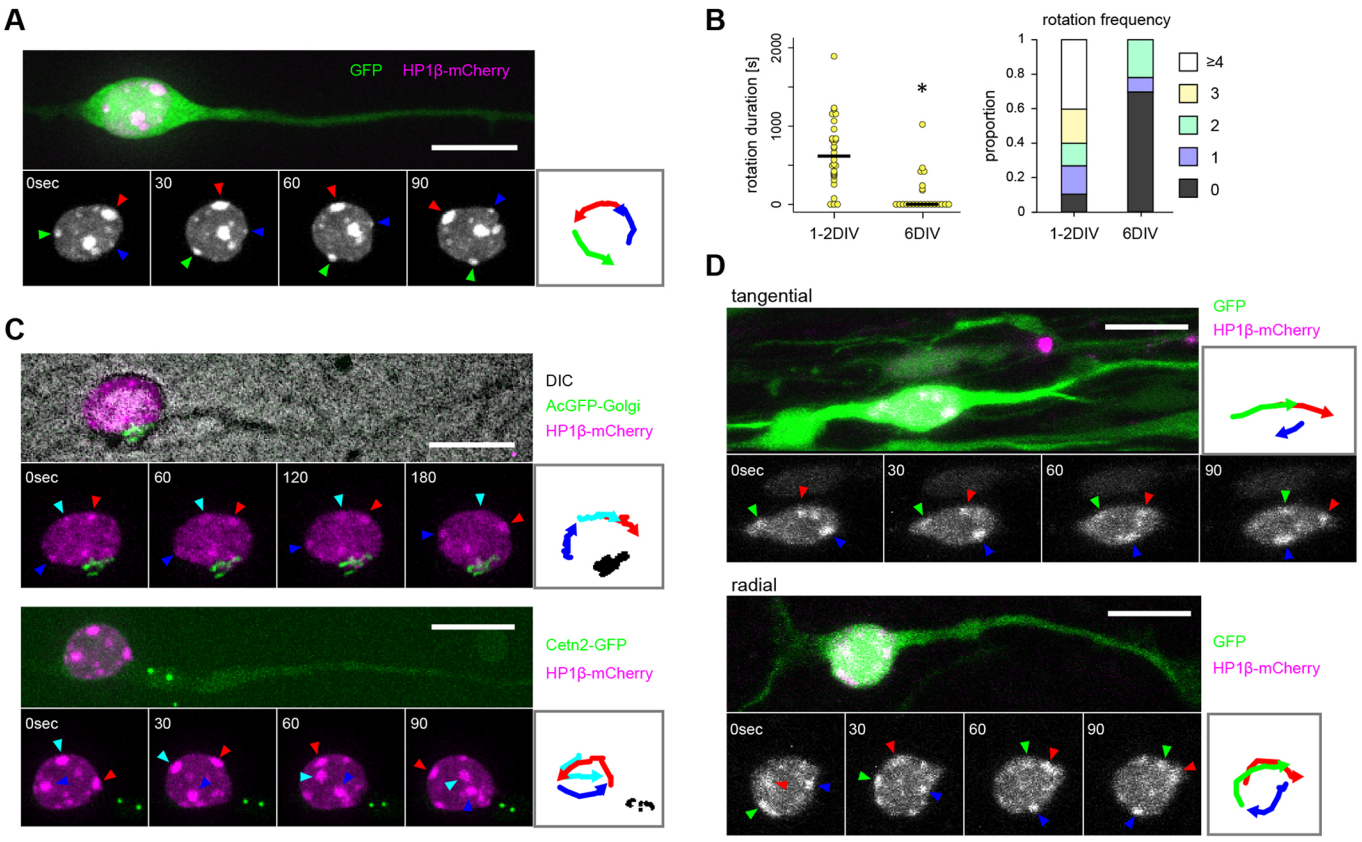

Fig. 1. The nucleus rotates in migrating GCGs. (A) Time-lapse sequences of a migrating CGC expressing GFP (green) and HP1β-mCherry (magenta) at 1 DIV (Movie 1). Colored arrowheads indicate the positions of HP1β spots. Trajectories of individual spots are shown on the right. (B) Duration (left; total rotation time per hour) and frequency (right; the number of rotation events per hour) of nuclear rotation in CGCs at 1-2 DIV and 6 DIV. Bars in dot plots indicate the median. n=30 for 1-2 DIV, n=23 for 6 DIV; *P<0.01, Kolmogorov–Smirnov test. (C) Time-lapse sequences of migrating CGCs expressing HP1β-mCherry (magenta) together with AcGFP-Golgi (green; top) or Cetn2-GFP (green; bottom) *in vitro*. Representative images from 12 and 10 cells observed in the respective conditions are shown. Colored arrowheads indicate the positions of HP1β spots. Trajectories of GFP-labeled Golgi apparatus and centrosome are traced in black, together with the HP1β spots, on the right. (Movie 3). (D) Time-lapse sequence of migrating CGCs expressing GFP (green) and HP1β-mCherry (magenta) during tangential (top) and radial (bottom) migration in organotypic slices. Representative images from 8 cells during tangential migration and 16 cells during radial migration are shown. Arrowheads indicate the positions of HP1β spots. Trajectories of individual spots are shown on the right (Movie 4). Scale bars: 10 µm.

motile neurons at 1-2 DIV (Fig. 1A,B). The nucleus spun clockwise or counterclockwise, and it occasionally switched rotation direction. By contrast, the nucleus in mature postmigratory neurons at 6 DIV was rather static and did not show notable rotation (Fig. 1B, Fig. S1B,C; Movie 1, right).

To determine whether only the nucleoplasmic compartments including heterochromatin or the entire nucleus including the nuclear envelope rotates, we visualized the nuclear envelope by transfecting mCherry-lamin B1. mCherry-lamin B1 was unevenly distributed on the nuclear membrane and allowed us to track rotation at a comparable speed to heterochromatin, suggesting that the nuclear interior and nuclear envelope rotated together as a unit (Fig. S1D, Movie 2).

We next examined whether other organelles associated with the nucleus rotate simultaneously. Cultured CGCs were co-transfected with either AcGFP-Golgi or centrin 2 (Cetn2)-GFP together with HP1β-mCherry to visualize the dynamics of the Golgi apparatus and the centrosome, respectively (Wu et al., 2015). The Golgi stacks juxtaposed to the nucleus in the cell soma (Fig. 1C). Unexpectedly, the Golgi was rather static during migration and stayed in the same position even when the nucleus underwent active rotation (Movie 3, left). Likewise, the centrosome did not follow nuclear spinning even though it moved dynamically in the cell soma during migration as previously reported (Umeshima et al., 2007) (Fig. 1C; Movie 3, right). These data suggest that the nuclear rotation is not driven by global cytoplasmic streaming but by a force that is applied specifically to the nucleus.

To verify whether the nuclear rotation is an artifact of isolated, free-moving neurons on a glass surface, we observed CGCs migrating in neural tissue in an organotypic slice of the cerebellum (Umeshima et al., 2007). HP1β-mCherry and GFP were electroporated in the primary fissures of postnatal day (P) 8 mice cerebella, and cerebellar slices were prepared at P10 when CGCs undergo tangential and radial migration. Time-lapse imaging using confocal microscopy revealed that the nucleus was drastically more deformed and underwent frequent rotation during both tangential and radial migration in brain tissue (Fig. 1D, Movie 4). This indicates that the nuclear rotation is a natural event in migrating neurons in the developing cerebellum.

Nuclear rotation is driven by the force for nuclear translocation

As nuclear rotation was observed only in migratory neurons, we hypothesized that the rotation was driven by the same force as that propelling nuclear translocation. Consistent with this hypothesis, nuclear rotation was frequently observed immediately before or after saltatory movement of the nucleus (Fig. 2A,B). Cytoplasmic dilations were observed at the proximal leading process, as previously

Development (2018) 145, dev158782. doi:10.1242/dev.158782

reported (Movie 1) (Tsai et al., 2007; Trivedi et al., 2017), while nuclear rotation was also seen in those lacking a typical dilation.

The driving force for nuclear movement must be applied to multiple points on the round surface of the nucleus, and displacement must be driven when the net force acts on the center of mass. On the other hand, biased forces must exert a torque and drive the nuclear rotation around an axis orthogonal to the direction of nuclear translocation (Fig. 2C). To prove our hypothesis, we determined the rotation axis and its angle to the direction of migration. The motion of the HP1β-mCherry spots was traced during rotation by three-dimensional particle tracking. The positions of the heterochromatin spots in each nucleus remained fixed relative to one another so that we were able to track their trajectories in real (*xyz*) space (Fig. S1C). In all cases examined, the rotation axis was nearly orthogonal to the leading process, which directs migration (mean angle to the leading process, 75.1°; Fig. 2D, E). On the other hand, unlike the flat nucleus in fibroblasts, which primarily rotates in two dimensions parallel to the substrate plane (Levy and Holzbaur, 2008), the oval nucleus in CGCs rotated in three dimensions with some bias toward the substrate plane (mean angle to the substrate plane, 57.5°; Fig. 2E, Fig. S1E). There was no bias, but frequent switches, between clockwise or counterclockwise rotation (Fig. 2E, Movie 5). The mean velocity of nuclear rotation was 47.1±3.4°/min, which is one order faster than those observed in other cell types, such as migrating fibroblasts (<10°/min) and developing muscle cells (<6°/min) (Capers, 1960; Paddock and Albrecht-Buehler, 1986; Ji et al., 2007; Levy and Holzbaur, 2008; Brosig et al., 2010; Wilson and Holzbaur, 2012). These results are consistent with our hypothesis that nuclear rotation is not a random event but is driven by a strong directional force towards the orientation of nuclear translocation.

We found that the nuclei actively rotated when they were spherical, whereas the non-rotating nuclei were more elongated in the direction of migration (Fig. 2F). Notably, moving nuclei were dynamically sharpened at their front, implying a point force applied to the anterior of the nuclear envelope (Fig. 2G, Movies 5 and 6). Thus, the tensile force of migration appears to cause nuclear strain energy that is converted to either anterior deformation, displacement, or rotation, depending on the nucleus shape and stress points. We thus utilized nuclear rotation as a new readout of the cytoskeletal forces driving nuclear migration.

Nesprins are indispensable for nuclear translocation and rotation

It has been shown that the LINC complex proteins nesprin-1 and -2 (Syne1 and Syne2) are directly involved in nuclear translocation by connecting the cytoskeleton and related motor proteins to the nuclear envelope (Zhang et al., 2009). Nesprins interact via the KASH domain with SUN proteins, which span the inner nuclear envelope and anchor to the nuclear lamina (Starr and Fischer, 2005). To examine whether nuclear rotation is driven by a cytoskeletal force mediated by the LINC complex, we transfected CGCs with a deletion mutant of nesprin-1 lacking the N-terminal cytoplasmic region (mCherry-KASH1), which is reported to inhibit the activity of endogenous nesprin-1/2 (Stewart-Hutchinson et al., 2008). Time-lapse imaging showed that overexpression of mCherry-KASH1 strongly inhibited nuclear rotation and, to a lesser extent, nuclear translocation (Fig. 3A-C, Movie 7). As a negative control, we also

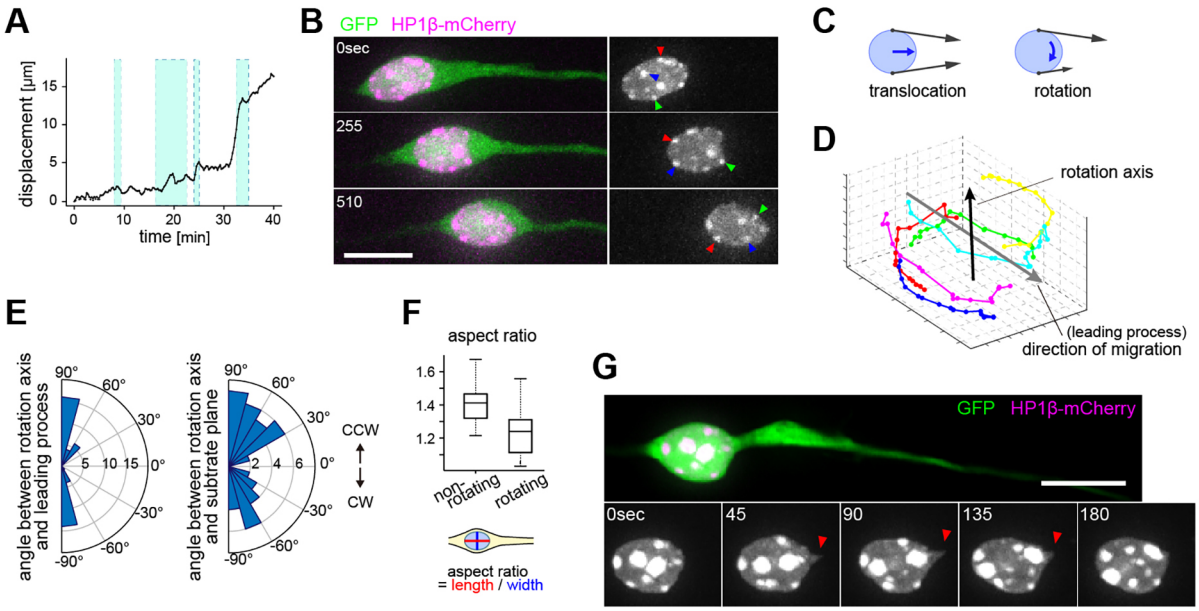

Fig. 2. The nucleus rotates toward the direction of its translocation. (A) Nuclear translocation and rotation in a migrating CGC plotted against time. The *y*-axis indicates the positions of the centroid of the nucleus. Blue shading indicates the time windows when nuclear rotation occurred. (B) Time-lapse sequence of a CGC that rotates during translocation. Colored arrowheads indicate HP1β spots. (C) Hypothetical schemes of force transmission during nuclear translocation and rotation. When cytoskeletal forces (gray arrows) are bilaterally balanced, the net force (blue arrow) drives nuclear translocation (left). Unbalanced cytoskeletal forces generate spin torques and drive nuclear rotation (right). (D) Representative traces of HP1β spots on the nuclear surface during rotation. Colored dots and lines indicate the trajectories of individual spots. Black arrow indicates the rotation axis calculated from the trajectories. Gray arrow indicates the direction of migration, i.e. the leading process. (E) Distribution of the angle of the rotation axis to the leading process (left) and to the substrate plane (right). Counterclockwise (CCW) and clockwise (CW) rotations are presented as positive and negative angles, respectively. *n*=45 events from 12 cells. (F) The aspect ratio (length/width) of the nucleus in non-rotating (rotation frequency of 0) and rotating (rotation frequency ≥5) cells. Aspect ratio was calculated for every frame of 1 h time-lapse images at 15 s intervals, and then averaged. *n*=10 cells for each group. Box plots with minimum to maximum whiskers include all data points. (G) Time-lapse sequence of a CGC expressing GFP (green) and HP1β-mCherry (magenta) *in vitro* (Movie 5). Arrowheads indicate the temporal sharp peak formed at the front of the nucleus. Scale bars: 10 μm.

Development (2018) 145, dev158782. doi:10.1242/dev.158782

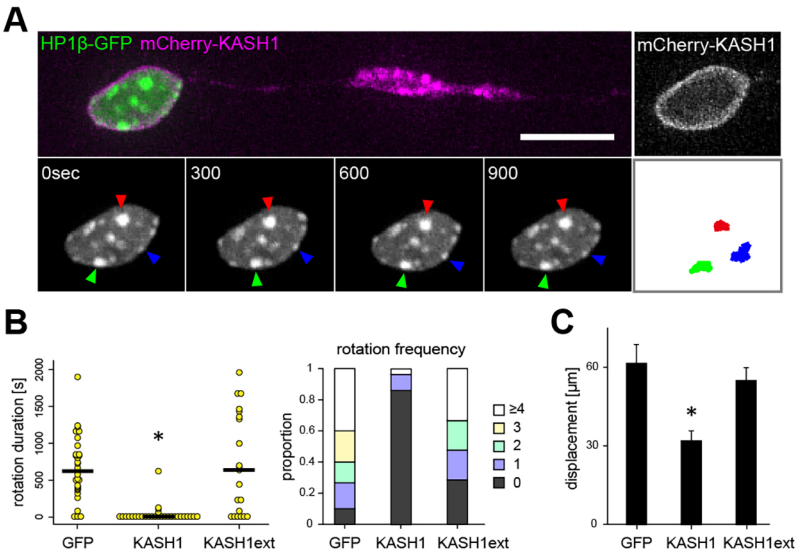

Fig. 3. Nesprin inhibition halts nuclear translocation and rotation. (A) Time-lapse sequences of CGCs expressing HP1β-GFP (green) with mCherry-KASH1 (magenta) *in vitro* (Movie 7). mCherry-KASH1 localizes in the nuclear envelope and endosomes as previously reported. Colored arrowheads indicate the positions of HP1β spots on the nuclear surface. Trajectories of individual spots are shown on the right. Scale bar: 10 µm. (B) Duration (left) and frequency (right) of nuclear rotations per hour in CGCs expressing the indicated constructs. Bars in the dot plots indicate the median. $n \geq 21$ for all data points; *$P<0.01$, Kolmogorov–Smirnov test. (C) Mean±s.e.m. displacements of nuclei during 5 h in CGCs expressing nesprin mutants. $n=60$ cells for each group; *$P<0.01$, *t*-test.

expressed mCherry-KASH1ext, which has additional C-terminal amino acids that do not bind to the cytoskeleton or interfere with the endogenous LINC complex (Stewart-Hutchinson et al., 2008). Overexpression of mCherry-KASH1ext did not affect nuclear rotation or translocation, indicating that inhibition of the LINC complex specifically interferes with rotation and translocation (Fig. 3B,C, Movie 7).

Actin and microtubules differentially regulate nuclear rotation and translocation

Nesprin-1/2 have been shown to interact with actin and the microtubule motors dynein and kinesin (Gerlitz and Bustin, 2011; Rajgor and Shanahan, 2013; Chang et al., 2015). To further identify the cytoskeletal systems involved in nuclear rotation, we examined the effect of cytoskeleton-disrupting agents. Treatment with the actin depolymerizer cytochalasin B (20 µM) immediately disrupted the actin cytoskeleton, as revealed by LifeAct-2xGFP transfected into migrating CGCs (Movie 8, left). Surprisingly, the nucleus actively rotated even after complete disruption of actin filaments, whereas nuclear translocation was strongly inhibited (Fig. 4A,B). We also confirmed that the nucleus stopped forward movement but continued spinning intermittently after treatment with blebbistatin (50 µM), a potent inhibitor of non-muscle myosin II (Fig. 4A,B). These results indicate that a contractile force of actomyosin is required for nuclear translocation, but not for rotation.

We next tested the effect of the microtubule depolymerizer nocodazole. Treatment with nocodazole (1 µM) disrupted microtubule filaments, as visualized by DCX-GFP expression (Fig. S2; Movie 8, right). Many of the nocodazole-treated cells sprouted exuberant protrusions and strongly agitated the cell soma, consistent with previous studies showing that nocodazole increases actin-based cell contractility via activation of the RhoA-ROCK-MLC pathway (Chang et al., 2008). Despite the increased cell motility, nuclear spinning was significantly attenuated after disrupting microtubule filaments with nocodazole (Fig. 4A). The directional translocation of the nucleus, in the forward direction, was also perturbed (Fig. 4B). We also tested the effect of the microtubule stabilizer taxol (5 µM) and found similar inhibition of nuclear translocation and rotation (Fig. 4A,B). These results suggest that nuclear rotation is associated with nuclear translocation driven by the microtubule-dependent force.

We further visualized microtubule dynamics during nuclear spinning by transfecting CGCs with DCX-GFP and HP1β-mCherry. We observed thick bundles of microtubules extending from the leading process toward the anterior surface of the nucleus, as reported previously (Umeshima et al., 2007). These microtubules were highly dynamic during neuronal migration, and some filaments appeared to closely associate with the nucleus and follow its rotation, supporting the idea that microtubules are directly associated with the rotating nucleus (Fig. 4C, Movie 9).

Microtubule motors serve as the driving force for nuclear rotation

It is widely accepted that cytoplasmic dynein is the predominant motor mediating the microtubule-dependent force during nucleokinesis in neuronal migration (Cooper, 2013). We investigated the involvement of cytoplasmic dynein in nuclear rotation by molecular perturbation of the two dynein adaptors Lis1 (Pafah1b1) and dynactin, which were previously shown to function in parallel to recruit dynein to the nucleus (Vallee et al., 2012). It has previously been shown that an N-terminal fragment of Lis1 (Lis1N), which has a dominant inhibitory effect on Lis1-dynein function, inhibits nuclear migration in neurons (Tsai et al., 2005; Umeshima et al., 2007). Overexpression of Lis1N significantly inhibited nuclear rotation in CGCs (Fig. 5A; Movie 10, left). Dynactin has been implicated in most dynein-mediated functions (Vallee et al., 2012). Dynactin function can be inhibited by overexpressing the first coiled-coil domain of the dynactin subunit $p150^{glued}$ (p150-CC1; also known as Dctn1) (Quintyne et al., 1999). CGCs transfected with p150-CC1 were altered in shape, with aberrant filopodia. Nuclear spinning was strongly inhibited in these cells (Fig. 5A; Movie 10, right). These results suggest that dynein is involved in the force that generates nuclear rotation.

Nesprin-2 has been shown to interact with kinesin light chain (KLC), which forms the kinesin-1 complex with the kinesin heavy chain Kif5 (Schneider et al., 2011; Wilson and Holzbaur, 2015). It is known that CGCs express three isoforms of Kif5 (Kif5A, B and C) and at least three isoforms of KLC (KLC1, 2 and 4), which share high similarity and are likely to complement each other's function (Brain Transcriptome Database, http://www.cdtdb.neuroinf.jp). Double immunofluorescence revealed that Kif5B is highly expressed in the leading process and cell body of migrating CGCs

Development (2018) 145, dev158782. doi:10.1242/dev.158782

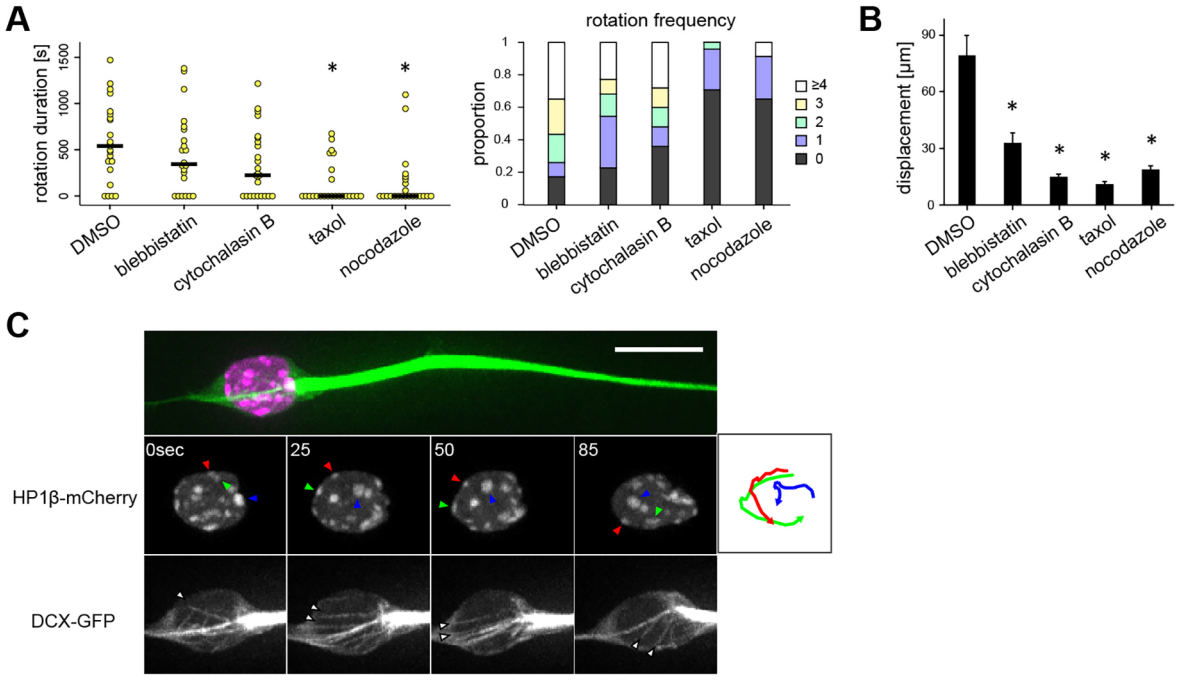

Fig. 4. Inhibition of actin and of microtubules differentially affect nuclear movements. (A) Duration (left) and frequency (right) of nuclear rotation per hour in CGCs treated with the indicated drugs. Bars in dot plots indicate median. $n \geq 22$ cells for all data points; *$P<0.01$, Kolmogorov–Smirnov test. (B) Mean±s.e.m. displacements of nuclei during 5 h in CGCs treated with the indicated drugs. $n=30$ cells for each group; *$P<0.01$, *t*-test. (C) Time-lapse sequences of a migrating CGC expressing DCX-GFP (green) and HP1β-mCherry (magenta) *in vitro* (Movie 9). Colored arrowheads indicate the positions of HP1β spots. Trajectories of individual spots are shown on the right. White arrowheads indicate the positions of the same microtubule bundles, which appear to be tilted to the direction of nuclear rotation. Scale bar: 10 μm.

in a partially overlapping, but non-identical, pattern with dynein (Fig. S3A). Strong signals were observed on the nuclear surface in cells permeabilized in a stringent buffer, suggesting that kinesin-1, as well as dynein, bound to the nuclear envelope in CGCs (Fig. S3B, C). The association of Kif5B with the nuclear envelope was further confirmed in a cell fractionation assay (Fig. S3D). Overexpression of mCherry-KASH1 abolished the Kif5B signals on the nuclear surface, suggesting that kinesin-1 binds to the nucleus via nesprin-1/2 (Fig. S3E,F). We therefore used a truncated mutant of Kif5B lacking the N-terminal motor domain (Kif5B-tail) as a dominant-

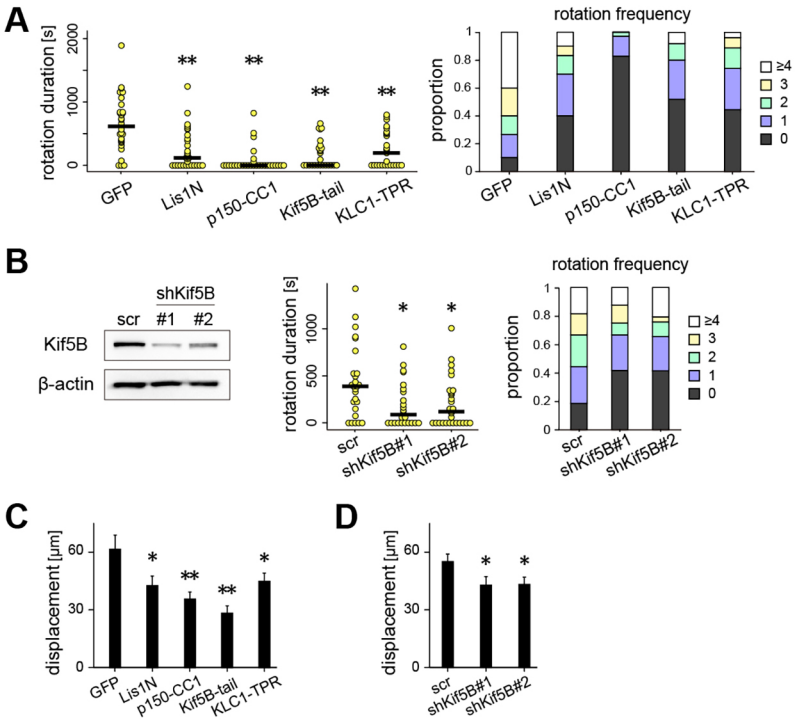

Fig. 5. Dynein and kinesin are involved in nuclear rotation. (A) Duration (left) and frequency (right) of nuclear rotation per hour in CGCs expressing dynein-inhibitor or kinesin-inhibitor constructs. Bars in dot plots indicate median. $n \geq 25$ for all data points; **$P<0.01$, Kolmogorov–Smirnov test. (B) Western blotting of NIH3T3 cells expressing the indicated shRNA constructs for Kif5B (left). scr, scramble control. Duration (middle) and frequency (right) of nuclear rotation per hour in CGCs transfected with the indicated shRNA constructs. Bars in dot plots indicate median. $n \geq 24$ for all data points; *$P<0.05$, Kolmogorov–Smirnov test. (C) Mean±s.e.m. displacements of nuclei during 5 h in CGCs expressing the indicated constructs. $n=60$ cells for each group; *$P<0.03$, **$P<0.01$, *t*-test. (D) Mean±s.e.m. displacements of nuclei during 5 h in CGCs expressing the indicated shRNA constructs. $n=80$ cells for each group; *$P<0.03$, *t*-test.

Development (2018) 145, dev158782. doi:10.1242/dev.158782

negative form to inhibit all three types of Kif5 (Coy et al., 1999; Konishi and Setou, 2009). Moderate GFP-Kif5B-tail overexpression indeed decreased the frequency of nuclear rotation in CGCs with little obvious change in cell polarity and shape (Fig. 5A, Fig. S4; Movie 11, left). ShRNA knockdown of Kif5B, the most abundant Kif5 subtype in the brain (Kanai et al., 2000), also suppressed nuclear rotation (Fig. 5B). To further verify the function of kinesin-1 in nuclear dynamics, we examined the effect of a dominant-negative mutant of KLC1 deleted of its heptad repeats that encompass the Kif5-binding domain (GFP-KLC1-TPR). KLC1-TPR is supposed to mask nesprins and to inhibit the binding of the kinesin-1 motor complex to the nucleus. As the immunofluorescence signal of KLC was not clear in CGCs, we used C2C12 cells and confirmed that GFP-KLC1-TPR accumulated on the nuclear surface and delocalized endogenous KLC1 to the cytoplasm (Fig. S5). Overexpression of GFP-KLC1-TPR reduced the rotation frequency of the nucleus, supporting the proposal that kinesin-1 drives nuclear motion by binding to nesprins (Fig. 5A; Movie 11, right). Molecular perturbation of dynein or kinesin-1 also suppressed nuclear translocation, consistent with the hypothesis that nuclear rotation is driven by the cytoskeletal force steering nuclear translocation (Fig. 5C,D). Together, these data strongly suggest that dynein and kinesin-1 mediate the microtubule-dependent forces that operate during nuclear rotation and translocation in CGCs.

The kinesin-binding domain of the cytoplasmic stretch of nesprin has been identified (Schneider et al., 2011). To investigate whether kinesin is sufficient for driving nuclear rotation, we overexpressed a nesprin-2 mutant deleted of its cytoplasmic region except for the four C-terminal spectrin repeats, which includes the kinesin-binding motif (nesp2-SR). We confirmed that GFP-nesp2-SR expressed in HEK293T cells bound to kinesin-1 but not dynein (Fig. S6). Overexpression of GFP-nesp2-SR induced a striking change in shape of the nucleus, with a constant sharp peak in the forward direction, which is seen only temporarily in normal cells (Fig. 6A, compare with Fig. 2G). However, rotation and translocation were downregulated in nesp2-SR-overexpressing cells, suggesting that binding of kinesin alone is insufficient to induce nuclear motion (Fig. 6B,C, Movie 12).

It is thought that most microtubules in migrating neurons originally emanate from the centrosome in front of the nucleus and align with their plus-end to the nucleus (Tanaka et al., 2004; Tsai et al., 2007). If the microtubules interact with the nucleus exclusively at their plus-ends, kinesins would be incapable of generating the plus-end motor activity. To explore the microtubule arrangement in migrating CGCs, we monitored the plus-ends of growing microtubules by transfecting GFP-tagged EB3 (Mapre3). We observed comet-like streaks of GFP-EB3 in the cell soma moving across the nucleus. In addition to the streaks, which emanate from the cell front toward the trailing process as previously reported (Tsai et al., 2007), a significant number of comets move toward the leading process (78.6% microtubules moving backward versus 21.4% microtubules moving forward, n=437 streaks from 17 cells; Fig. 6D). This is consistent with recent studies that identified a considerable fraction of non-centrosomal microtubules in migrating CGCs (Rao et al., 2016). These parallel and antiparallel microtubules were not segregated in distinct areas but were mixed in the perinuclear region (Fig. 6D, Movie 13).

CGC migration during cerebellar cortex formation requires kinesin-1

Finally, we investigated whether kinesin-1 is required for the migration of CGCs *in vivo*, as kinesin motor activity has never been implicated in nucleokinesis in postmitotic neurons. GFP-Kif5B-tail or control GFP was electroporated into immature granule neurons in the external granular layer (EGL) of the P8 mouse cerebellum. Injected brains were fixed and sectioned at P11 to assess neuronal migration from the EGL to the internal granular layer (IGL). The large majority of GFP-transfected CGCs finished migration in the

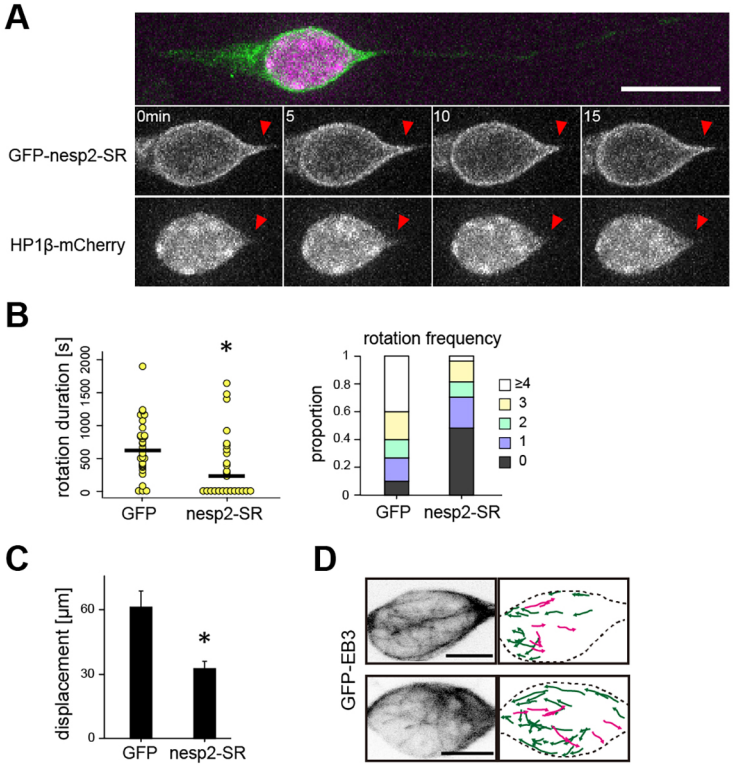

Fig. 6. Excess binding of kinesin and nesprin disrupts nuclear shape and movement. (A) Time-lapse sequence of a CGC expressing GFP-nesp2-SR (green) and HP1β-mCherry (magenta) *in vitro* (Movie 12). Arrowheads indicate the persistent sharp peak formed at the front of the nucleus. Scale bar: 10 µm (B) Duration (left) and frequency (right) of nuclear rotation per hour in CGCs expressing GFP or GFP-nesp2-SR. Bars in dot plots indicate the median. n≥27 for all data points; *P<0.01, Kolmogorov–Smirnov test. (C) Mean± s.e.m. displacements of nuclei during 5 h in CGCs expressing GFP-nesp2-SR. n=60 for each group; *P<0.01, t-test. (D) Organization and orientation of microtubules in migrating CGCs as demarcated by GFP-EB3. Image pairs show representative GFP-EB3 signals and individual microtubule trajectories tracked from 150 s time-lapse images (3 s intervals) (Movie 13). Colored arrows indicate the EB3 streaks moving backward (green) and forward (magenta) across the nucleus. Scale bars: 5 µm.

Development (2018) 145, dev158782. doi:10.1242/dev.158782

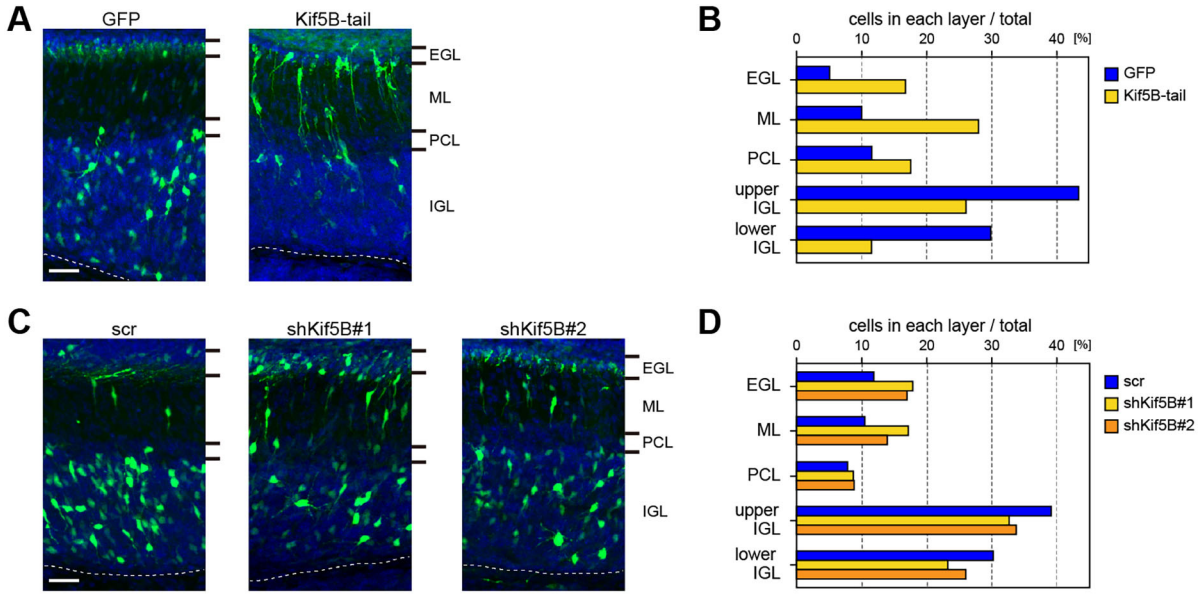

Fig. 7. Kinesin inhibition disrupts granule cell migration *in vivo*. (A) CGCs in the P8 mouse external granular layer (EGL) were electroporated with GFP or GFP-Kif5B-tail (green). Sagittal sections were made at P11. The EGL, molecular layer (ML), Purkinje cell layer (PCL) and internal granular layer (IGL) were identified by DAPI staining (blue). Dashed line indicates the border between the IGL and white matter. (B) The percentage of CGCs transduced with GFP or GFP-Kif5B-tail located in each layer. IGL was divided into upper and lower halves. *n*=709 cells from three brains for GFP, *n*=364 cells from three brains for GFP-Kif5B-tail; *P*<0.01, Chi-squared test. (C) CGCs in the P7 mouse EGL were electroporated with shRNA for Kif5B or scramble control (green). Sagittal sections were prepared at P10. The layers were identified by DAPI staining (blue). (D) The percentages of CGCs transfected with scramble (scr), shKif5B#1 or shKif5B#2 located in each layer. IGL was divided into upper and lower halves. *n*=662 cells from three brains for scramble, *n*=592 cells from three brains for shKif5B#1, and *n*=685 cells from three brains for shKif5B#2; *P*<0.01 for scramble versus shKif5B#1 or shKif5B#2, Chi-squared test. Scale bars: 30 µm.

IGL (73.3%), except for a small number of cells that remained in the EGL (5.1%) or molecular layer (ML) (10.0%) (Fig. 7A,B). By contrast, transfection with GFP-Kif5B-tail significantly increased the number of CGCs that remained in the EGL (16.8%) and ML (28.0%), at the expense of those reaching the IGL (37.6%). Inhibition of Kif5B by shRNA knockdown also significantly retarded CGC migration *in vivo* (Fig. 7C,D). These results indicate that kinesin-1 is involved in the generation of cytoskeletal force driving nuclear rotation and translocation in migrating CGCs during cerebellum development.

DISCUSSION

In this study, a fine spatiotemporal analysis of nuclear behavior reveals highly dynamic movements of the nucleus, including intermittent fast rotation, in newly born CGCs. In contrast to fibroblast nuclear migration driven by a direct link between nesprins and actin (Luxton et al., 2010; Bergert et al., 2015), our results implicate the interaction of nesprins and microtubules in the nuclear rotation of migrating CGCs. While microtubules in migrating neurons are highly dynamic, they essentially align parallel to the force vector of rotation along the direction of the leading process (Fig. 4C, Fig. 6D, Movie 13) (Tsai et al., 2007; Umeshima et al., 2007). We observed dynamic peaking of the front of the nucleus during migration, which is enhanced by the excess interaction of nesprin and kinesin-1 (Movies 5 and 12). These observations support the idea that microtubule motors are directly anchored to the LINC complex, applying a point force to the nuclear envelope and triggering nuclear deformation and rotation. Whereas nuclear rotation is solely dependent on microtubule motors, nuclear translocation requires both actomyosin and microtubule motors. Previous studies have demonstrated that the actomyosin in the leading process generates the traction force pulling the nucleus in CGCs (He et al., 2010; Jiang et al., 2015), and this actomyosin tethers perinuclear microtubules and transmits the contractile force to the microtubules (Trivedi et al., 2017). We thus surmise that the point force of microtubules and associated motors are responsible for steering the nucleus during rotation and deformation, while the strong contractile force of actomyosin synergistically drives nuclear translocation by acting on a large area of the nucleus and/or regulating microtubule positioning in CGCs.

It is widely accepted that minus-end motor activity of dynein plays a major role in nuclear migration in postmitotic neurons (Cooper, 2013). Perinuclear microtubules are thought to orient uniformly with their minus-ends toward the cell front, excluding a major role of the plus-end-directed kinesin in forward nuclear motion. One exception is bi-directional interkinetic nuclear migration in cortical neural stem cells, which is driven apically by dynein and basally by kinesin-3 (Tsai et al., 2010; Carabalona et al., 2016). Here we demonstrate that perinuclear microtubules are of mixed polarity and both dynein and kinesin-1 are involved in directional nuclear motion in the postmitotic neuron. It has been shown that kinesin indirectly regulates nuclear migration by recruiting dynein to the nuclear surface (Yamada et al., 2010), by regulating neuronal polarity (Falnikar et al., 2013), or by promoting transport and secretion of neurotrophins (Carabalona et al., 2016). By contrast, our data suggest that kinesin motor activity drives nuclear motion directly through interaction with the LINC complex. How do the opposing motors cooperatively drive unidirectional nuclear motion? It is unlikely that dynein and kinesin are segregated by microtubules of opposite polarity and always generate the same vector force. We observed frequent switches of rotation direction, suggesting a dynamic interaction of the opposing motors with nesprins driving both forward and backward movement of the nucleus. Consistently, overexpression of nesprin with only the

Development (2018) 145, dev158782. doi:10.1242/dev.158782

kinesin-binding domain induces persistent nuclear deformation while inhibiting rotation and translocation. Given that microtubule polarity is strongly biased toward those with the minus-end to the cell front, dynein on these dominant microtubules is considered to be the major player in nuclear translocation, while kinesin may enhance nuclear rotation and smooth translocation (Fig. S7).

We observed that the nucleus shows remarkable deformation during migration in dense neural tissues in organotypic slice cultures. Such nuclear deformation is seen in various cell migration events, such as hematopoiesis, metastasis and inflammation, and is due to local compression of the cell during passage through narrow regions of interstitial tissue or basement membrane (Wolf et al., 2007, 2013; Shin et al., 2013). Recent studies have indicated that kinesin-1 and cytoplasmic dynein are anchored to the LINC complex and synergistically regulate the nuclear migration through narrow constrictions in *C. elegans* embryos (Fridolfsson and Starr, 2010; Bone et al., 2016). Nuclear rotation is likely to be a consequence of unbalanced point forces exerted by the microtubule motors that pull the nucleus through constrictions. Dynamic changes in the cytoskeletal arrangement caused by the rotation might sometimes optimize the positioning of the nucleus and the cytoskeletons, and thus enable smooth translocation in the crowded neural tissue. Alternatively, rotation may release the excess force and thereby protect the nucleus from damage due to extreme deformation toward the narrow constrictions (Denais et al., 2016; Raab et al., 2016).

Given the apparent diversity of cytoskeletal organization among neuronal species, the nuclear dynamics and regulatory mechanism must be analyzed comparatively in other neurons to obtain a better understanding of the physiology and pathology of nucleokinesis in the brain.

MATERIALS AND METHODS

Animals

ICR mice were obtained from Japan SLC. All experiments involving mice were approved by the Animal Experimentation Committee of Kyoto University, and were performed in accordance with its guidelines.

cDNA constructs

pAcGFP1-Golgi was obtained from Clontech. pCAG-EGFP, pCentrin2-EGFP and pCAG-DsRed2-Nuc were constructed as previously described (Umeshima et al., 2007). pCAG-LifeAct-2xGFP was created by insertion of the LifeAct sequence fused with tandemly duplicated EGFP into pCAGGS vector. HP1β-mCherry and HP1β-GFP were created by cloning heterochromatin protein 1 beta from a mouse brain cDNA library fused with mCherry or EGFP at the C-terminus. For mCherry-KASH1, nesprin-1 cDNA (8726-8799 aa) was amplified and fused with mCherry at the N-terminus. mCherry-KASH1ext was created by fusing an additional C-terminal stretch (VDGTAGPGSTGSR peptide derived from pEGFP-C1) into mCherry-KASH1. mCherry-lamin B1, DCX-GFP, and GFP-EB3 were created by insertion of lamin B1, doublecortin and EB3 cDNAs cloned from a mouse brain cDNA library into pCAGGS. EGFP or mCherry sequence was inserted at the N- or C-terminus of respective cDNAs. GFP-Lis1N (1-87 aa of Lis1), GFP-p150-CC1 (214-548 aa of $p150^{Glued}$), GFP-Kif5B-tail (808-963 aa of Kif5B), GFP-KLC1-TPR (187-499 aa of KLC1), and GFP-nesp2-SR (6231-6874 aa of nesprin-2) were amplified and fused with EGFP at the N-terminus. For RNAi experiments, target sequences for mouse Kif5B 5′-GCATATTTCTTATTAATGTAA-3′ (shKif5B#1) and 5′-GGATAAAGATATTGCTATTAC-3′ (shKif5B#2) were cloned into the pBAsi-mU6 vector (TAKARA). The promotor and shRNA sequence regions were excised and inserted into pCAG-EGFP.

CGC culture, subcellular fractionation and immunostaining

Reaggregate cultures of CGCs were prepared as previously described with a few modifications (Kawaji et al., 2004). Cerebella from P4-6 ICR mice of either sex were dissociated and incubated in a cocktail containing 4-8 µg plasmid DNA and 6 µl Lipofectamine 2000 (Invitrogen) for 6-8 h to make reaggregates. The resulting reaggregates were plated on glass-based dishes coated with poly-D-lysine and laminin and maintained in Basal Medium Eagle (BME) with 26.4 mM glucose, 25 mM sodium bicarbonate, 1% bovine serum albumin (BSA), 1× N-2 supplement (Thermo Fisher Scientific) and penicillin-streptomycin at 37°C/5% CO_2.

Migrating CGCs in reaggregated cultures were immunostained for kinesin, dynein or tubulin and imaged as described in the supplementary Materials and Methods. Nuclear and cytosolic fractions from dissociated cerebella of P4 ICR mice were prepared for western analysis as described in the supplementary Materials and Methods.

Time-lapse imaging

Reaggregate cultures were observed with an incubation imaging system (LCV100, Olympus) through a 20× objective (N.A. 0.7), or with a spinning-disk confocal microscope (CV1000, Yokogawa) through a 20× objective (N.A. 0.75) and a 100× oil-immersion objective (N.A. 1.3) at 37°C with 5% CO_2 flow. For nuclear rotation analysis, time-lapse images were obtained every 15 s for 1 h to trace the trajectories of HP1β spots. For translocation analysis, images were obtained every 5 min for 5 h to measure the cumulative distance of directional travel of the nucleus. For drug treatments, half of the culture medium was replaced with pre-warmed fresh medium containing blebbistatin (50 µM; Sigma), cytochalasin B (20 µM; Sigma), taxol (5 µM; Sigma) or nocodazole (1 µM; Sigma) dissolved in DMSO. For imaging of migration in organotypic slice cultures, cerebella were dissected and embedded in 3% agarose 2 days after electroporation, and sectioned into 300 µm-thick coronal slices with a vibratome. Slices placed on Millicell-CM (Millipore) were mounted in collagen gel and soaked in medium (60% BME, 25% Earle's Balanced Salt, 15% horse serum, 3 mM L-glutamine, 1 mM sodium pyruvate, 31 mM glucose, 21.4 mM sodium bicarbonate, 1× N-2 supplement). The tissue was kept in an incubator chamber attached to an upright microscope stage (BX61WI, Olympus) at 37°C with 85% O_2/5% CO_2 flow. Images were obtained with a laser-scanning confocal microscope (FV1000, Olympus) every 15 or 30 s through a 60× water-immersion objective (N.A. 1.1).

In vivo electroporation and image acquisition

P7 or P8 mice were anesthetized on ice and injected with plasmid DNAs diluted in Tris-EDTA buffer (pH 8.0) with a 33-gauge needle connected to the anode. Tweezer-type electrodes connected to the cathode were placed on the occipital regions. Six electric pulses of 70 mV for 50 ms duration were applied with 150 ms intervals using a CUY21 (Nepagene). The pups were revived at 37°C and returned to the litter. Electroporated mouse brains were isolated at P10 or P11 and fixed with 4% PFA in PBS. The cerebella were then sectioned into 100 µm-thick sagittal slices with a vibratome and stained with DAPI. Images were acquired with the FV1000 through a 20× objective (N.A. 0.75).

C2C12 culture and western blotting

C2C12 cells were cultured, induced to myogenic differentiation, immunostained for KLC1 and GFP, and imaged as described in the supplementary Materials and Methods.

NIH3T3 cell culture and western blotting

NIH3T3 (RCB1862, RIKEN BRC) cells were maintained at 37°C/5% CO_2 in D-MEM with 10% fetal bovine serum and penicillin-streptomycin. shRNA constructs were transfected with Nucleofector II (Lonza) program U-030. After 2.5 days of transfection, cells were harvested in lysis buffer [50 mM Tris-HCl pH 7.4, 75 mM sodium chloride, 2.5 mM magnesium chloride, 1 mM EDTA, 0.1% Triton X-100, 1× protease inhibitor cocktail (Thermo Fisher)]. Lysates were subjected to SDS-PAGE and western blotting with the following antibodies (see also supplementary Materials and Methods): rabbit anti-Kif5B (1:1000; ab167429, Abcam), HRP-conjugated anti-rabbit IgG (1:10,000; 170-6515, Bio-Rad) and HRP-conjugated mouse anti-β-actin (1:10,000; sc-47778, Santa Cruz). For HEK293T cell culture and western blotting, see the supplementary Materials and Methods.

Quantitative analysis of nuclear rotation

Nuclear rotation was defined as rotation of HP1β spots of more than 15° over a period of at least 1 min. For one rotation event, trajectories of several HP1β-mCherry spots were tracked in three-dimensional time-lapse images using TrackMate (Tinevez et al., 2016). Principal component analysis was performed on the three-dimensional data of each trajectory to determine the best fitting plane. The axis of rotation was calculated by averaging the normal vectors of each fitted plane. The angle between the rotation axis and the direction of migration was calculated in the range of 0 to 90°. The *z*-component of the direction of migration was set 0.

Statistical analyses

The duration of nuclear rotation was compared using the Kolmogorov–Smirnov test. *In vivo* migration was compared using the chi-squared test. $P<0.05$ was considered statistically significant. Nuclear translocation was compared using a left-tailed *t*-test with $P<0.03$ considered significant.

Acknowledgements

We thank Professor M. Kaneko (Osaka University) and his lab members for invaluable discussions; Mr F. Ishidate for technical assistance; and Professor D. Packwood for critical reading of the manuscript.

Competing interests

The authors declare no competing or financial interests.

Author contributions

Conceptualization: H.U., M.K.; Formal analysis: Y.K.W.; Investigation: Y.K.W., H.U., J.K.; Writing - original draft: Y.K.W., M.K.

Funding

This work was supported by the KAKENHI of the Japan Society for the Promotion of Science (JSPS) to M.K. (#16H06484, #26290005) and H.U. (#26830012, #26106715), and by the JSPS Fellowship for Young Scientists to Y.K.W. (#16J11143).

Supplementary information

Supplementary information available online at
http://dev.biologists.org/lookup/doi/10.1242/dev.158782.supplemental

References

Bellion, A., Baudoin, J. P., Alvarez, C., Bornens, M. and Métin, C. (2005). Nucleokinesis in tangentially migrating neurons comprises two alternating phases: forward migration of the Golgi/centrosome associated with centrosome splitting and myosin contraction at the rear. *J. Neurosci.* **25**, 5691-5699.

Bergert, M., Erzberger, A., Desai, R. A., Aspalter, I. M., Oates, A. C., Charras, G., Salbreux, G. and Paluch, E. K. (2015). Force transmission during adhesion-independent migration. *Nat. Cell Biol.* **17**, 524-529.

Bone, C. R., Chang, Y.-T., Cain, N. E., Murphy, S. P. and Starr, D. A. (2016). Nuclei migrate through constricted spaces using microtubule motors and actin networks in *C. elegans* hypodermal cells. *Development* **143**, 4193-4202.

Brosig, M., Ferralli, J., Gelman, L., Chiquet, M. and Chiquet-Ehrismann, R. (2010). Interfering with the connection between the nucleus and the cytoskeleton affects nuclear rotation, mechanotransduction and myogenesis. *Int. J. Biochem. Cell Biol.* **42**, 1717-1728.

Capers, C. R. (1960). Multinucleation of skeletal muscle in vitro. *J. Biophys. Biochem. Cytol.* **7**, 559-566.

Carabalona, A., Hu, D. J.-K. and Vallee, R. B. (2016). KIF1A inhibition immortalizes brain stem cells but blocks BDNF-mediated neuronal migration. *Nat. Neurosci.* **19**, 253-262.

Chang, Y.-C., Nalbant, P., Birkenfeld, J., Chang, Z.-F. and Bokoch, G. M. (2008). GEF-H1 couples nocodazole-induced microtubule disassembly to cell contractility via RhoA. *Mol. Biol. Cell* **19**, 2147-2153.

Chang, W., Worman, H. J. and Gundersen, G. G. (2015). Accessorizing and anchoring the LINC complex for multifunctionality. *J. Cell Biol.* **208**, 11-22.

Cooper, J. A. (2013). Cell biology in neuroscience: mechanisms of cell migration in the nervous system. *J. Cell Biol.* **202**, 725-734.

Coy, D. L., Hancock, W. O., Wagenbach, M. and Howard, J. (1999). Kinesin's tail domain is an inhibitory regulator of the motor domain. *Nat. Cell Biol.* **1**, 288-292.

Crisp, M., Liu, Q., Roux, K., Rattner, J. B., Shanahan, C., Burke, B., Stahl, P. D. and Hodzic, D. (2006). Coupling of the nucleus and cytoplasm: role of the LINC complex. *J. Cell Biol.* **172**, 41-53.

Denais, C. M., Gilbert, R. M., Isermann, P., McGregor, A. L., te Lindert, M., Weigelin, B., Davidson, P. M., Friedl, P., Wolf, K. and Lammerding, J. (2016). Nuclear envelope rupture and repair during cancer cell migration. *Science* **352**, 353-358.

Dialynas, G. K., Makatsori, D., Kourmouli, N., Theodoropoulos, P. A., McLean, K., Terjung, S., Singh, P. B. and Georgatos, S. D. (2006). Methylation-independent binding to histone H3 and cell cycle-dependent incorporation of HP1β into heterochromatin. *J. Biol. Chem.* **281**, 14350-14360.

Falnikar, A., Tole, S., Liu, M., Liu, J. S. and Baas, P. W. (2013). Polarity in migrating neurons is related to a mechanism analogous to cytokinesis. *Curr. Biol.* **23**, 1215-1220.

Fridolfsson, H. N. and Starr, D. A. (2010). Kinesin-1 and dynein at the nuclear envelope mediate the bidirectional migrations of nuclei. *J. Cell Biol.* **191**, 115-128.

Gerlitz, G. and Bustin, M. (2011). The role of chromatin structure in cell migration. *Trends Cell Biol.* **21**, 6-11.

He, M., Zhang, Z.-H., Guan, C.-B., Xia, D. and Yuan, X.-B. (2010). Leading tip drives soma translocation via forward F-actin flow during neuronal migration. *J. Neurosci.* **30**, 10885-10898.

Hu, D. J.-K., Baffet, A. D., Nayak, T., Akhmanova, A., Doye, V. and Vallee, R. B. (2013). Dynein recruitment to nuclear pores activates apical nuclear migration and mitotic entry in brain progenitor cells. *Cell* **154**, 1300-1313.

Ji, J. Y., Lee, R. T., Vergnes, L., Fong, L. G., Stewart, C. L., Reue, K., Young, S. G., Zhang, Q., Shanahan, C. M. and Lammerding, J. (2007). Cell nuclei spin in the absence of lamin B1. *J. Biol. Chem.* **282**, 20015-20026.

Jiang, J., Zhang, Z.-H., Yuan, X.-B. and Poo, M.-M. (2015). Spatiotemporal dynamics of traction forces show three contraction centers in migratory neurons. *J. Cell Biol.* **209**, 759-774.

Kanai, Y., Okada, Y., Tanaka, Y., Harada, A., Terada, S. and Hirokawa, N. (2000). KIF5C, a novel neuronal kinesin enriched in motor neurons. *J. Neurosci.* **20**, 6374-6384.

Kawaji, K., Umeshima, H., Eiraku, M., Hirano, T. and Kengaku, M. (2004). Dual phases of migration of cerebellar granule cells guided by axonal and dendritic leading processes. *Mol. Cell. Neurosci.* **25**, 228-240.

Konishi, Y. and Setou, M. (2009). Tubulin tyrosination navigates the kinesin-1 motor domain to axons. *Nat. Neurosci.* **12**, 559-567.

Levy, J. R. and Holzbaur, E. L. F. (2008). Dynein drives nuclear rotation during forward progression of motile fibroblasts. *J. Cell Sci.* **121**, 3187-3195.

Luxton, G. W. G., Gomes, E. R., Folker, E. S., Vintinner, E. and Gundersen, G. G. (2010). Linear arrays of nuclear envelope proteins harness retrograde actin flow for nuclear movement. *Science* **329**, 956-959.

Manzini, M. C. and Walsh, C. A. (2011). What disorders of cortical development tell us about the cortex: one plus one does not always make two. *Curr. Opin. Genet. Dev.* **21**, 333-339.

Martini, F. J. and Valdeolmillos, M. (2010). Actomyosin contraction at the cell rear drives nuclear translocation in migrating cortical interneurons. *J. Neurosci.* **30**, 8660-8670.

Moon, H. M. and Wynshaw-Boris, A. (2013). Cytoskeleton in action: lissencephaly, a neuronal migration disorder. Wiley Interdiscip. *Rev. Dev. Biol.* **2**, 229-245.

Paddock, S. W. and Albrecht-Buehler, G. (1986). Distribution of microfilament bundles during rotation of the nucleus in 3T3 cells treated with monensin. *Exp. Cell Res.* **163**, 525-538.

Quintyne, N. J., Gill, S. R., Eckley, D. M., Crego, C. L., Compton, D. A. and Schroer, T. A. (1999). Dynactin is required for microtubule anchoring at centrosomes. *J. Cell Biol.* **147**, 321-334.

Raab, M., Gentili, M., de Belly, H., Thiam, H.-R., Vargas, P., Jimenez, A. J., Lautenschlaeger, F., Voituriez, R., Lennon-Duménil, A.-M., Manel, N. et al. (2016). ESCRT III repairs nuclear envelope ruptures during cell migration to limit DNA damage and cell death. *Science* **352**, 359-362.

Rajgor, D. and Shanahan, C. M. (2013). Nesprins: from the nuclear envelope and beyond. *Expert Rev. Mol. Med.* **15**, e5.

Rao, A. N., Falnikar, A., O'Toole, E. T., Morphew, M. K., Hoenger, A., Davidson, M. W., Yuan, X. B. and Baas, P. W. (2016). Sliding of centrosome-unattached microtubules defines key features of neuronal phenotype. *J. Cell Biol.* **213**, 329-341.

Schaar, B. T. and McConnell, S. K. (2005). Cytoskeletal coordination during neuronal migration. *Proc. Natl. Acad. Sci. USA* **102**, 13652-13657.

Schneider, M., Lu, W., Neumann, S., Brachner, A., Gotzmann, J., Noegel, A. A. and Karakesisoglou, I. (2011). Molecular mechanisms of centrosome and cytoskeleton anchorage at the nuclear envelope. *Cell. Mol. Life Sci.* **68**, 1593-1610.

Shin, J.-W., Spinler, K. R., Swift, J., Chasis, J. A., Mohandas, N. and Discher, D. E. (2013). Lamins regulate cell trafficking and lineage maturation of adult human hematopoietic cells. *Proc. Natl. Acad. Sci. USA* **110**, 18892-18897.

Shinohara, R., Thumkeo, D., Kamijo, H., Kaneko, N., Sawamoto, K., Watanabe, K., Takebayashi, H., Kiyonari, H., Ishizaki, T., Furuyashiki, T. et al. (2012). A role for mDia, a Rho-regulated actin nucleator, in tangential migration of interneuron precursors. *Nat. Neurosci.* **15**, 373-380.

Shu, T., Ayala, R., Nguyen, M.-D., Xie, Z., Gleeson, J. G. and Tsai, L.-H. (2004). Ndel1 operates in a common pathway with LIS1 and cytoplasmic dynein to regulate cortical neuronal positioning. *Neuron* **44**, 263-277.

Solecki, D. J., Trivedi, N., Govek, E.-E., Kerekes, R. A., Gleason, S. S. and Hatten, M. E. (2009). Myosin II motors and F-actin dynamics drive the coordinated movement of the centrosome and soma during CNS glial-guided neuronal migration. *Neuron* **63**, 63-80.

Starr, D. A. and Fischer, J. A. (2005). KASH 'n Karry: The KASH domain family of cargo-specific cytoskeletal adaptor proteins. *BioEssays* **27**, 1136-1146.

Stewart-Hutchinson, P. J., Hale, C. M., Wirtz, D. and Hodzic, D. (2008). Structural requirements for the assembly of LINC complexes and their function in cellular mechanical stiffness. *Exp. Cell Res.* **314**, 1892-1905.

Tanaka, T., Serneo, F. F., Higgins, C., Gambello, M. J., Wynshaw-Boris, A. and Gleeson, J. G. (2004). Lis1 and doublecortin function with dynein to mediate coupling of the nucleus to the centrosome in neuronal migration. *J. Cell Biol.* **165**, 709-721.

Tinevez, J.-Y., Perry, N., Schindelin, J., Hoopes, G. M., Reynolds, G. D., Laplantine, E., Bednarek, S. Y., Shorte, S. L. and Eliceiri, K. W. (2016). TrackMate: an open and extensible platform for single-particle tracking. *Methods* **115**, 80-90.

Trivedi, N. and Solecki, D. J. (2011). Neuronal migration illuminated: a look under the hood of the living neuron. *Cell Adhes. Migr.* **5**, 42-47.

Trivedi, N., Stabley, D. R., Cain, B., Howell, D., Laumonnerie, C., Ramahi, J. S., Temirov, J., Kerekes, R. A., Gordon-Weeks, P. R. and Solecki, D. J. (2017). Drebrin-mediated microtubule-actomyosin coupling steers cerebellar granule neuron nucleokinesis and migration pathway selection. *Nat. Commun.* **8**, 14484.

Tsai, J.-W., Chen, Y., Kriegstein, A. R. and Vallee, R. B. (2005). LIS1 RNA interference blocks neural stem cell division, morphogenesis, and motility at multiple stages. *J. Cell Biol.* **170**, 935-945.

Tsai, J.-W., Bremner, K. H. and Vallee, R. B. (2007). Dual subcellular roles for LIS1 and dynein in radial neuronal migration in live brain tissue. *Nat. Neurosci.* **10**, 970-979.

Tsai, J.-W., Lian, W.-N., Kemal, S., Kriegstein, A. R. and Vallee, R. B. (2010). Kinesin 3 and cytoplasmic dynein mediate interkinetic nuclear migration in neural stem cells. *Nat. Neurosci.* **13**, 1463-1471.

Umeshima, H., Hirano, T. and Kengaku, M. (2007). Microtubule-based nuclear movement occurs independently of centrosome positioning in migrating neurons. *Proc. Natl. Acad. Sci. USA* **104**, 16182-16187.

Vallee, R. B., Seale, G. E. and Tsai, J.-W. (2009). Emerging roles for myosin II and cytoplasmic dynein in migrating neurons and growth cones. *Trends Cell Biol.* **19**, 347-355.

Vallee, R. B., McKenney, R. J. and Ori-McKenney, K. M. (2012). Multiple modes of cytoplasmic dynein regulation. *Nat. Cell Biol.* **14**, 224-230.

Wilson, M. H. and Holzbaur, E. L. F. (2012). Opposing microtubule motors drive robust nuclear dynamics in developing muscle cells. *J. Cell Sci.* **125**, 4158-4169.

Wilson, M. H. and Holzbaur, E. L. F. (2015). Nesprins anchor kinesin-1 motors to the nucleus to drive nuclear distribution in muscle cells. *Development* **142**, 218-228.

Wolf, K., Wu, Y. I., Liu, Y., Geiger, J., Tam, E., Overall, C., Stack, M. S. and Friedl, P. (2007). Multi-step pericellular proteolysis controls the transition from individual to collective cancer cell invasion. *Nat. Cell Biol.* **9**, 893-904.

Wolf, K., te Lindert, M., Krause, M., Alexander, S., te Riet, J., Willis, A. L., Hoffman, R. M., Figdor, C. G., Weiss, S. J. and Friedl, P. (2013). Physical limits of cell migration: control by ECM space and nuclear deformation and tuning by proteolysis and traction force. *J. Cell Biol.* **201**, 1069-1084.

Wu, Y. K., Fujishima, K. and Kengaku, M. (2015). Differentiation of apical and basal dendrites in pyramidal cells and granule cells in dissociated hippocampal cultures. *PLoS ONE* **10**, e0118482.

Yamada, M., Toba, S., Takitoh, T., Yoshida, Y., Mori, D., Nakamura, T., Iwane, A. H., Yanagida, T., Imai, H., Yu-Lee, L. Y. et al. (2010). mNUDC is required for plus-end-directed transport of cytoplasmic dynein and dynactins by kinesin-1. *EMBO J.* **29**, 517-531.

Zhang, X., Lei, K., Yuan, X., Wu, X., Zhuang, Y., Xu, T., Xu, R. and Han, M. (2009). SUN1/2 and Syne/Nesprin-1/2 complexes connect centrosome to the nucleus during neurogenesis and neuronal migration in mice. *Neuron* **64**, 173-187.

Supplementary Figures

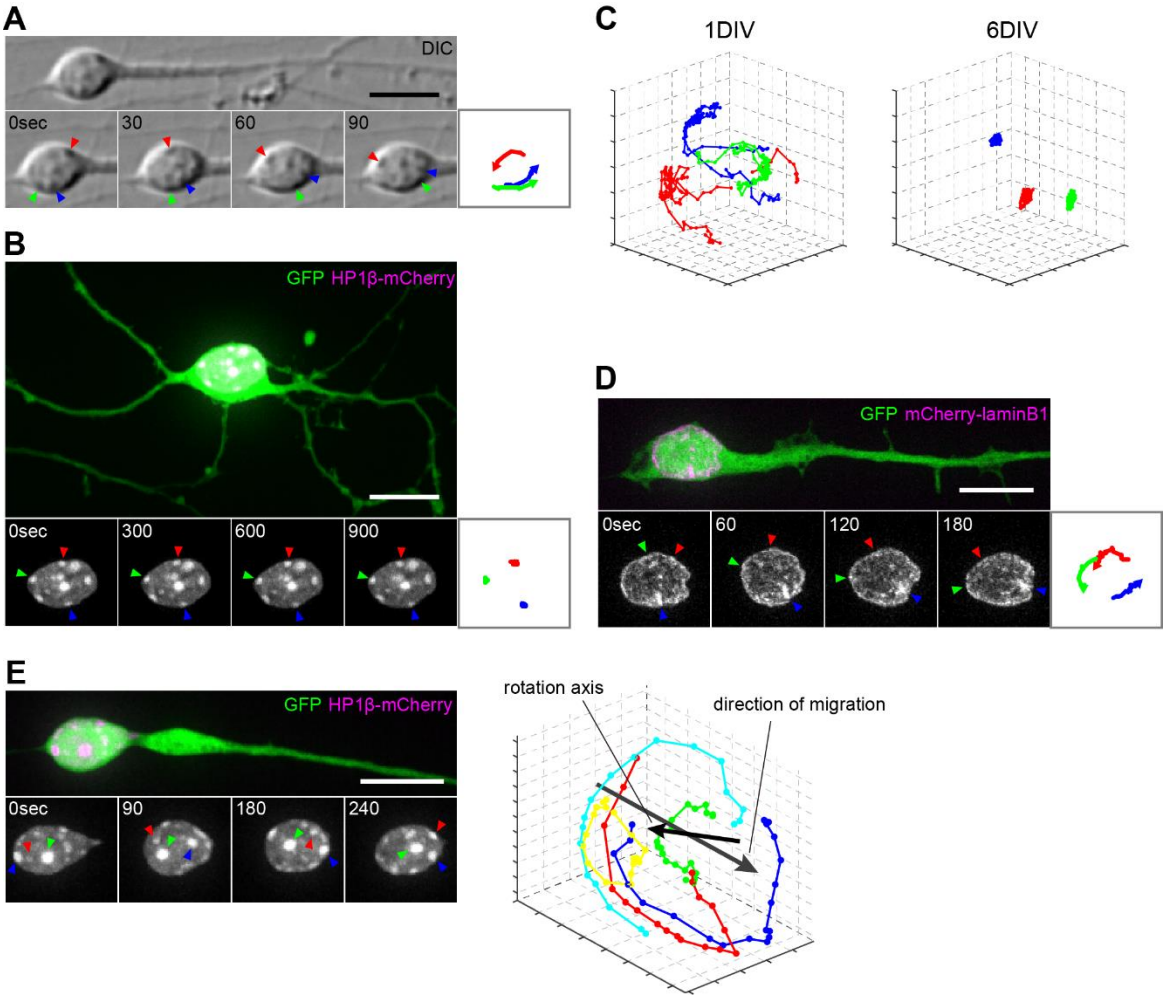

Fig. S1. The nucleus rotates in migrating cerebellar granule cell (A) Time-lapse sequence of DIC images of a migrating CGC in vitro. Colored arrowheads indicate the positions of nucleoli. Trajectories of individual nucleoli are shown in the right-most panel. (B) Time-lapse sequences of a post-migration CGC expressing GFP (green) and HP1β-mCherry (magenta) at 6 DIV (Movie 1). Colored arrowheads indicate the positions of HP1β spots on the nuclear surface. Trajectories of individual spots are shown in the right-most panels. (C) 3D plots of 30-min trajectories of HP1β-mCherry spots in the nucleus of a migrating CGC at 1 DIV and post-migratory CGC at 6 DIV. Positions of the HP1β-mCherry spots were detected from reconstructed 3D images and tracked at 15-sec intervals. Colored dots and lines indicate the trajectories of individual spots. Spots show

dynamic and coordinated motion in migrating CGCs, while they remain stationary at the same relative positions in post-migratory CGCs. (D) Time-lapse sequence of a CGC expressing GFP (green) and mCherry-laminB1 (magenta) in vitro. Colored arrowheads indicate the positions of laminB1 spots. (Movie 2). (E) Time-lapse sequence of a nucleus rotating around an axis parallel to the substrate plane (*left*) and 3D plots of the trajectories of HP1β-mCherry spots (*right*). Scale bars: 10 μm

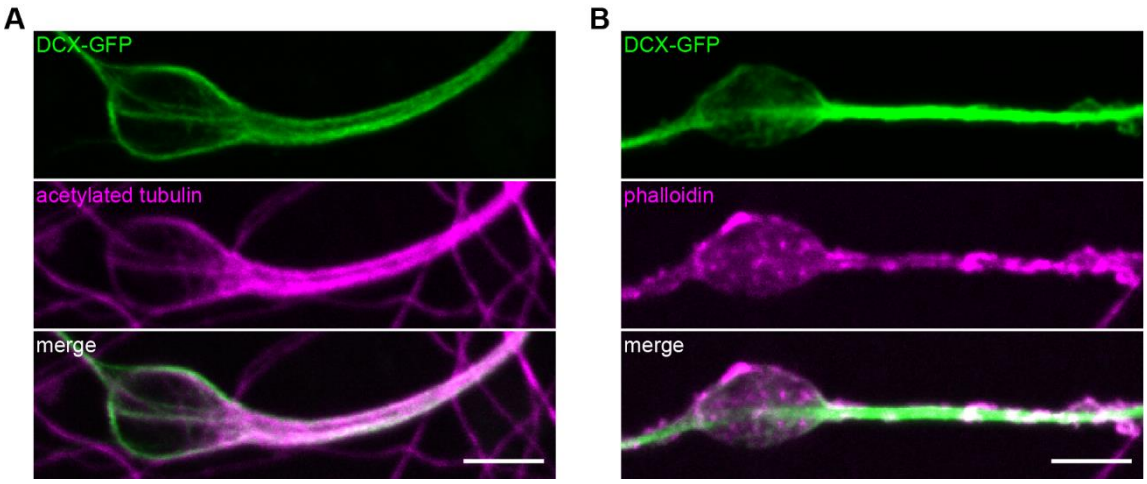

Fig. S2. DCX-GFP co-localizes with microtubules but not with actin. (A) Representative images of a CGC expressing DCX-GFP (green) fixed with methanol, and stained with acetylated tubulin (magenta). (B) Representative images of a CGC expressing DCX-GFP (green) fixed with PFA, and stained with Rhodamine-phalloidin (magenta). Scale bars: 5 μm

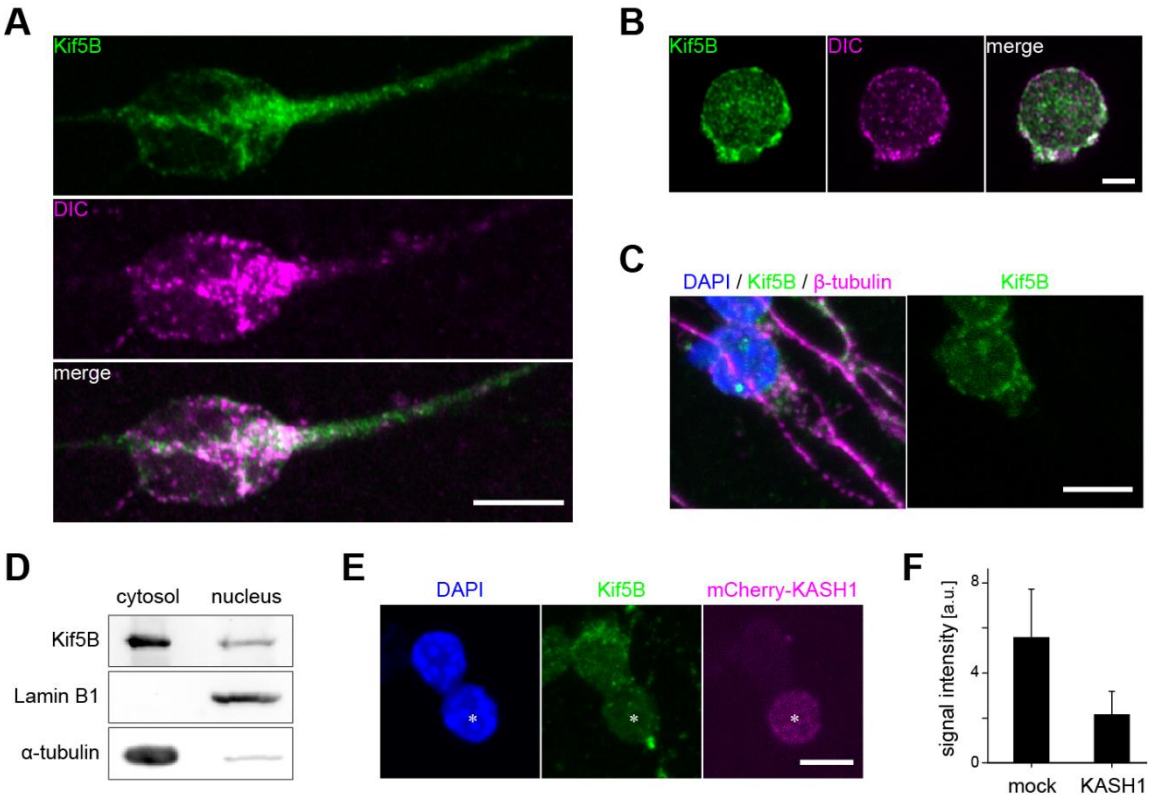

Fig. S3. Distribution of Kif5B and dynein in CGCs. (A) Super-resolution images of a migrating CGC stained with Kif5B (green) and dynein intermediate chain (magenta). Kinesin and dynein signals partially overlap. Scale bar: 5 μm. (B) Super-resolution images of a migrating CGC treated with hypotonic buffer. Kinesin (green) and dynein (magenta) signals partially overlap on the nuclear envelope. Scale bar: 2 μm. (C) Immunostaining of migrating CGCs with Kif5B (green) and β–tubulin (magenta). Nucleus was labeled with DAPI (blue). Multicolor image (left) shows a z-projection, while Kif5B image (right) shows a single section. Scale bar: 5 μm. (D) Subcellular localization of Kif5B in CGCs. Cerebella from P4 mice were fractionated into cytosolic and nuclear fractions that were then subjected to western blotting with indicated antibodies. Kif5B signal was detected in both the cytosol and nucleus. (E) Kif5B staining (green) in a CGC expressing mCherry-KASH1 (magenta). Asterisk indicates the transfected cell. Nucleus was labeled with DAPI (blue). Scale bar: 5 μm. (F) Quantification of Kif5B signal on the nuclear envelope in the CGCs transfected with either mock or mCherry-KASH1. n = 10 cells for each group; mean±s.e.m.

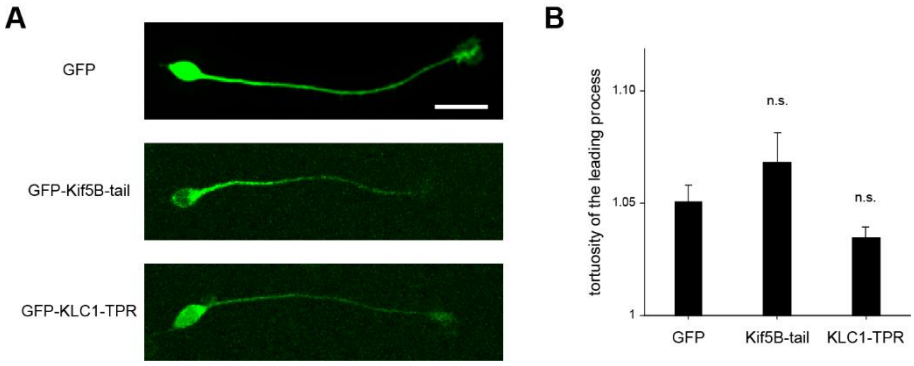

Fig. S4. Inhibition of kinesin-1 by overexpressing dominant-negative mutants does not affect cell morphology. (A) Representative images of CGCs expressing GFP, GFP-Kif5B-tail, or GFP-KLC1-TPR. Scale bar: 20 μm. (B) Quantification of the morphology of the leading process. The tortuosity was defined as L/d, where L is the length of the leading process, and d is the distance between the ends of the leading process. n = 30 cells for each group; mean±s.e.m. ; $p>0.05$, t-test.

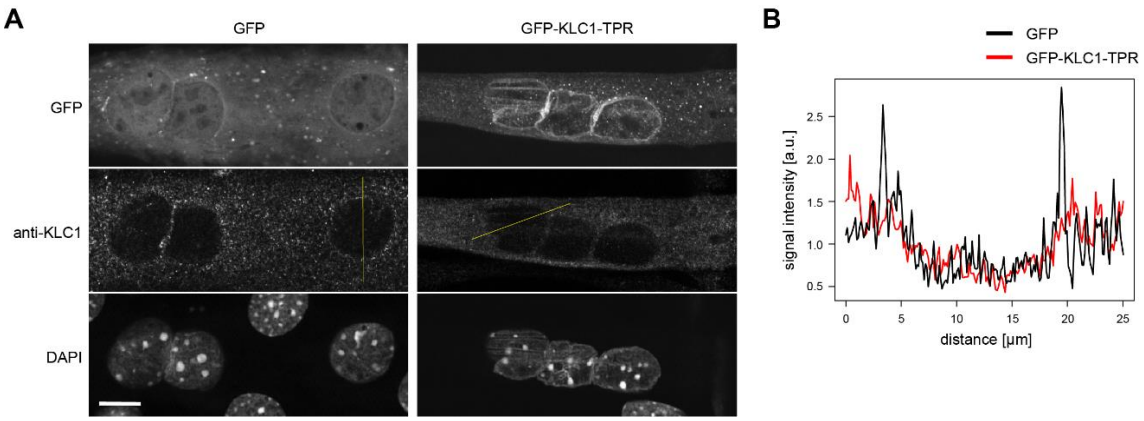

Fig. S5. KLC1-TPR overexpression delocalizes endogenous KLC1 from the nuclear envelope (A) Representative images of differentiated C2C12 cells expressing control GFP (left) or GFP-KLC1-TPR (right). Endogenous KLC1 was stained with an anti-KLC1 antibody that does not recognize GFP-KLC1-TPR. Scale bar: 10 µm. (B) The signal intensity of KLC1 immunofluorescence along the diameter of the nucleus (yellow lines in A). Signal peaks were observed on the nuclear envelope in GFP-expressing cells, while it disappeared in the cells expressing GFP-KLC1-TPR.

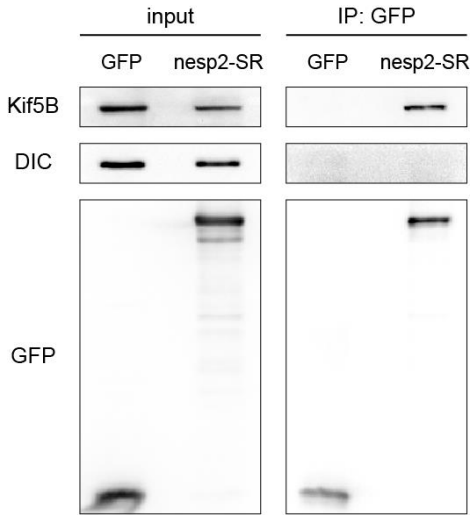

Fig. S6. GFP-nesp2-SR interacts with kinesin but not with dynein. Co-immunoprecipitation of HEK293T cells expressing GFP or GFP-nesp2-SR with anti-GFP. GFP-nesp2-SR precipitated Kif5B but not DIC.

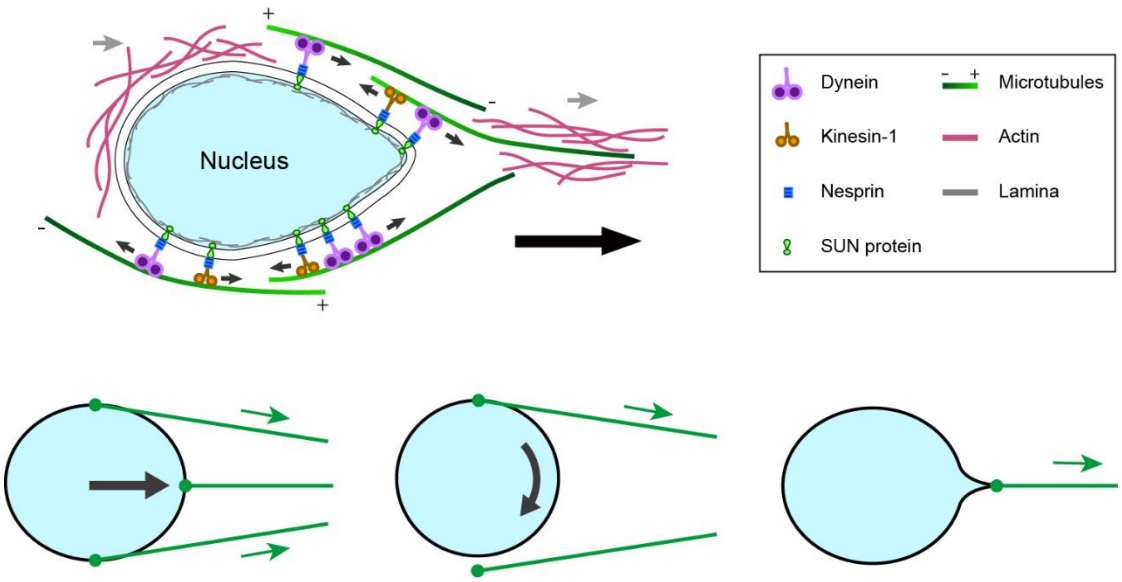

Fig. S7. Model of cytoskeletal control of nuclear dynamics in CGCs. The nucleus migrates toward the leading process (*right*). Dynamic arrays of parallel (minus-end to leading process) and fewer antiparallel (minus-end to trailing process) microtubules cover the nuclear envelope. Dynein and kinesin interact with nesprins at the nuclear envelope and generate a point force toward both anterior and posterior directions, which may drive frequent switches of rotation direction. Dynein along the parallel microtubules may serve as the predominant motor and cause net displacement toward the leading process. Actomyosin-based force may function independently of nesprins during nuclear translocation. Nuclear translocation, rotation, and deformation are induced depending on the positions of microtubule-dependent force.

Supplementary Movies

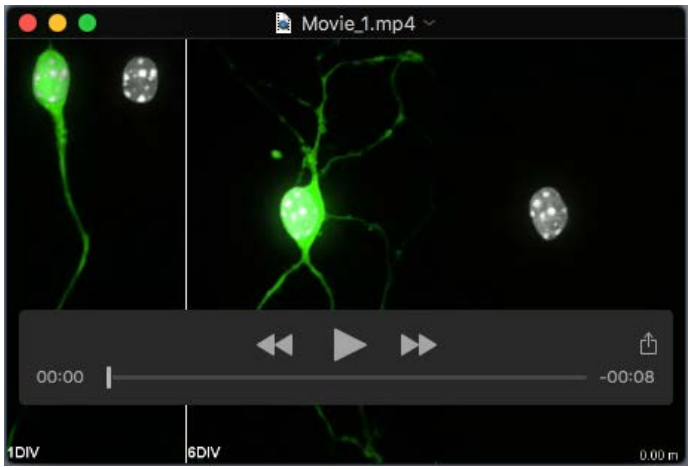

Movie 1. Nuclear dynamics of a migrating and a post-migratory CGC in vitro. Time-lapse movies of a CGC expressing GFP (green) and HP1β-mCherry (magenta) at 1 DIV (*left*) or 6 DIV (*right*). Images were acquired every 15 sec for 1 hr.

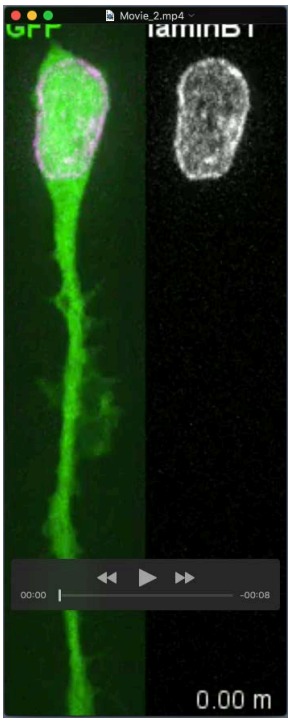

Movie 2. Dynamics of the nuclear envelope labeled with laminB1 in a migrating CGC in vitro. Time-lapse movie of a CGC expressing GFP (green) and mCherry-laminB1 (magenta) in vitro. Images were acquired every 15 sec for 1 hr.

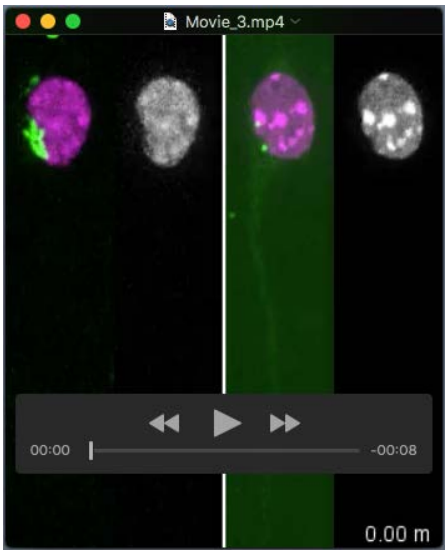

Movie 3. Dyanimcs of the Golgi apparatus and centrosome in migrating CGCs in vitro. Time-lapse movies of CGCs expressing HP1β-mCherry (magenta) together with AcGFP-Golgi (green; *left*) or Cetn2-GFP (green; *right*) in vitro. Images were acquired every 15 sec for 1 hr.

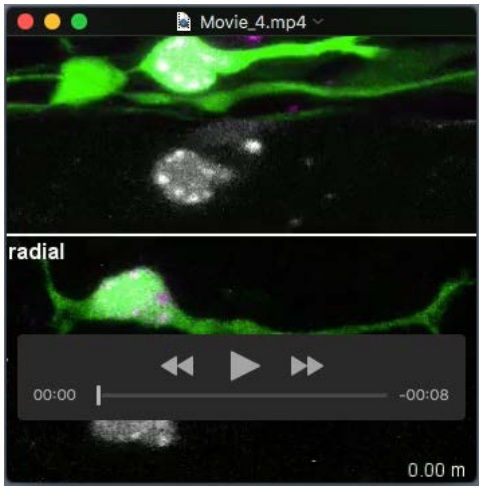

Movie 4. Nuclear dynamics of migrating CGCs in an organotypic slice. Time-lapse movies of tangential (*upper*) or radial (*lower*) migration of a CGC expressing GFP (green) and HP1β-mCherry (magenta) in an organotypic slice. Images were acquired every 30 sec (tangential) or 15 sec (radial) for 1 hr.

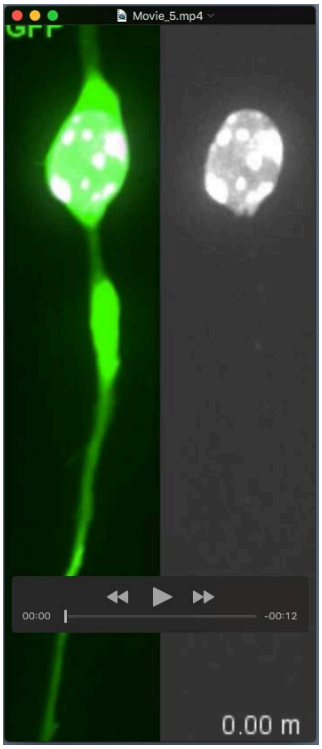

Movie 5. Sharp peaks temporarily formed in the nuclear envelope of a migrating CGC. Time-lapse movie of a CGC expressing GFP (green) and HP1β-mCherry (magenta) in vitro. Images were acquired every 15 sec for 1 hr.

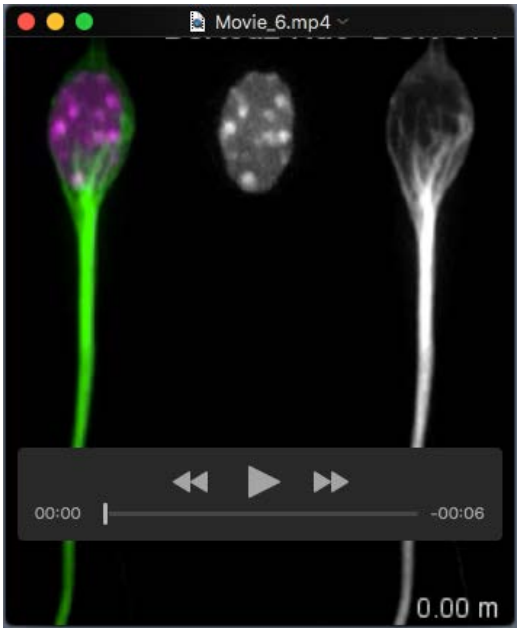

Movie 6. Nuclear shape change during translocation and rotation in a migrating CGC. Time-lapse movie of a CGC expressing DCX-GFP (green) and DsRed2-Nuc (magenta) in vitro. Images were acquired every 15 sec for 1 hr.

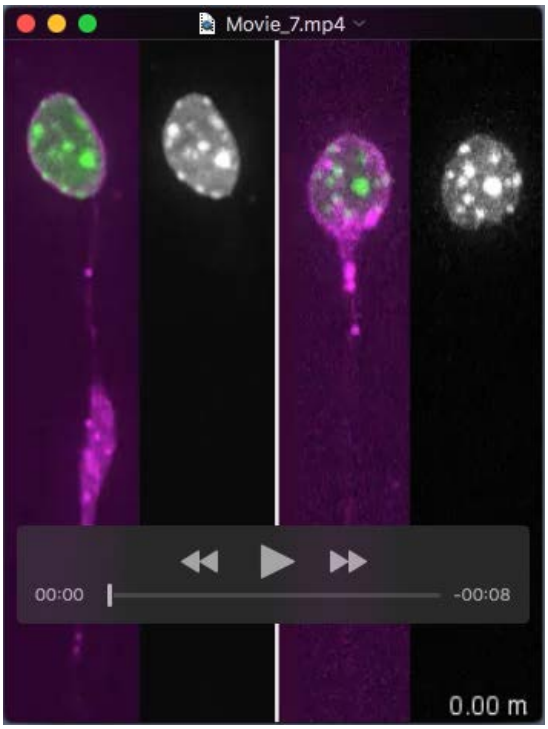

Movie 7. Dominant negative inhibition of KASH domain proteins affects the nuclear dynamics of CGCs. Time-lapse movies of CGCs expressing HP1β-GFP (green) together with mCherry-KASH1 (magenta; *left*) or mCherry-KASH1ext (magenta; *right*) in vitro. Images were acquired every 15 sec for 1 hr.

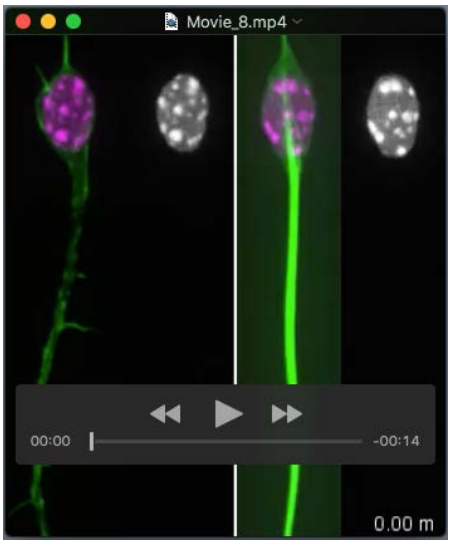

Movie 8. Nuclear dynamics of CGCs treated with drugs. Time-lapse movies of a CGC expressing HP1β-mCherry (magenta) together with LifeAct-2xGFP (green; *left*) or DCX-GFP (green; *right*). The cell was treated with 20 µM cytochalasin B (*left*) or 1 µM nocodazole (*right*). Images were acquired every 15 sec for 40 min (before drug treatment) and 1 hr (after drug treatment).

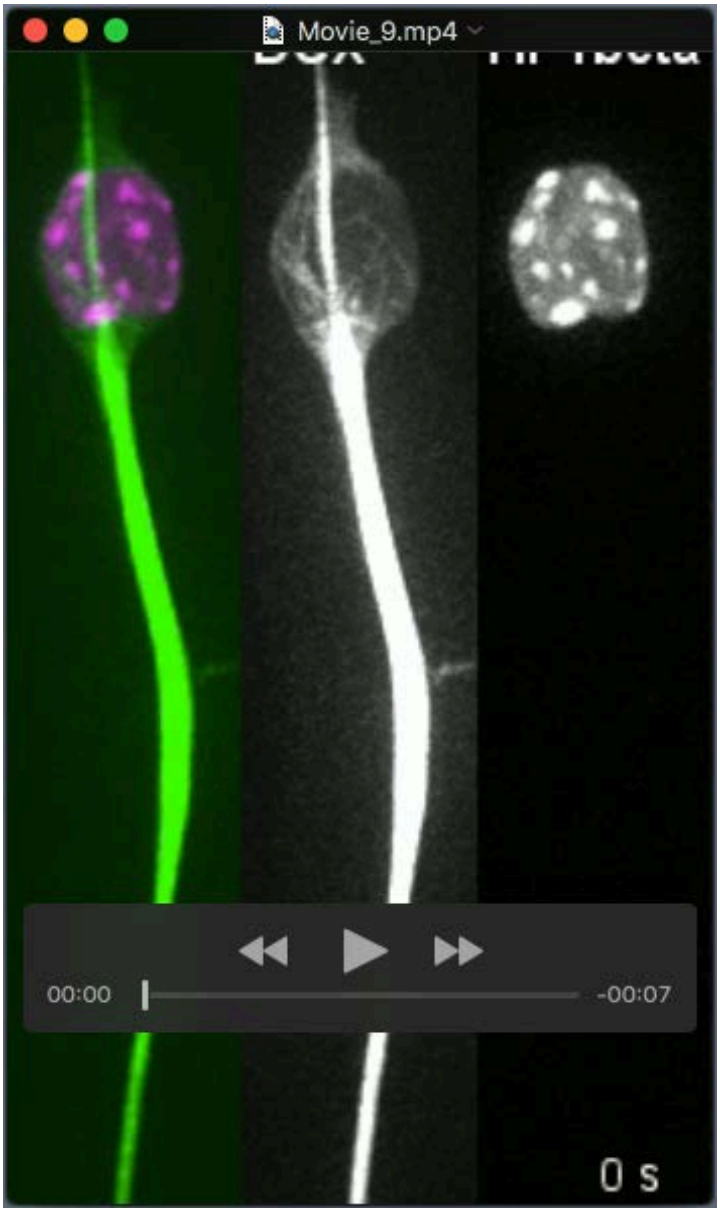

Movie 9. Microtubule dynamics during nuclear rotation. Time-lapse movie of a CGC expressing DCX-GFP (green) and HP1β-mCherry (magenta) in vitro. Images were acquired every 15 sec for 525 sec.

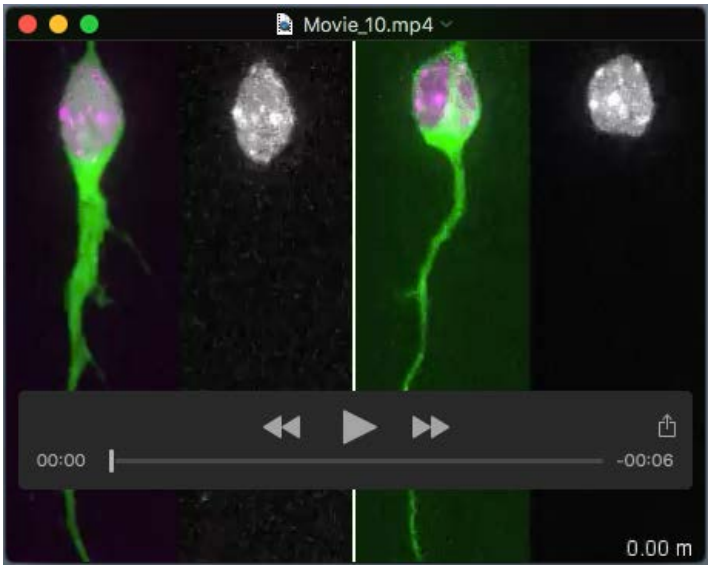

Movie 10. Inhibition of dynein by dominant negative Lis1 or p150^{Glued} affects the nuclear dynamics of CGCs. Time-lapse movies of CGCs expressing HP1β-mCherry (magenta) toghether with GFP-Lis1N (green; *left*) or GFP-p150-CC1 (green; *right*). Images were acquired every 15 sec for 1 hr.

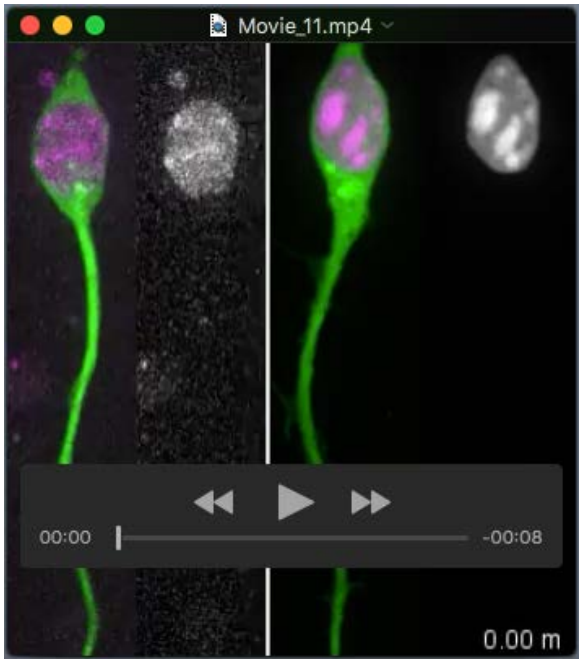

Movie 11. Inhibition of kinesin-1 by dominant negative Kif5 or KLC affects the nuclear dynamics of CGCs. Time-lapse movies of CGCs expressing HP1β-mCherry (magenta) together with GFP-Kif5B-tail (green; *left*) or GFP-KLC1-TPR (green; *right*). Images were acquired every 15 sec for 1 hr.

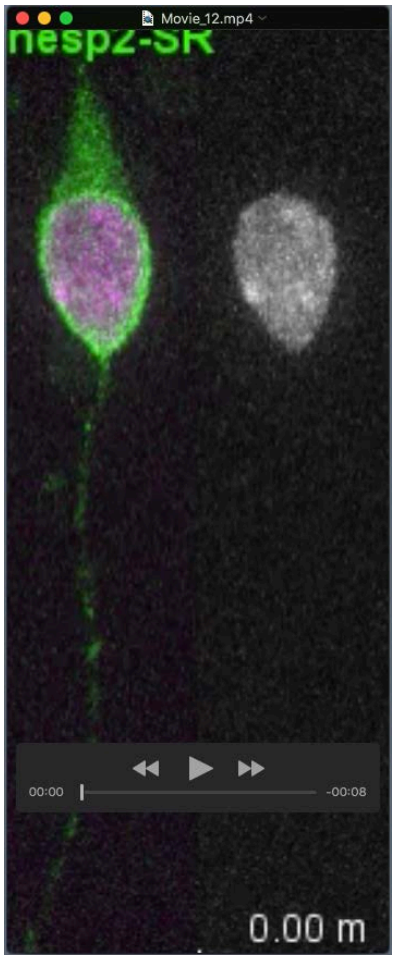

Movie 12. Nuclear dynamics of a CGC expressing a kinesin-binding nesprin mutant. Time-lapse movie of a CGC expressing GFP-nesp2-SR (green) and HP1β-mCherry (magenta) in vitro. Images were acquired every 15 sec for 1 hr.

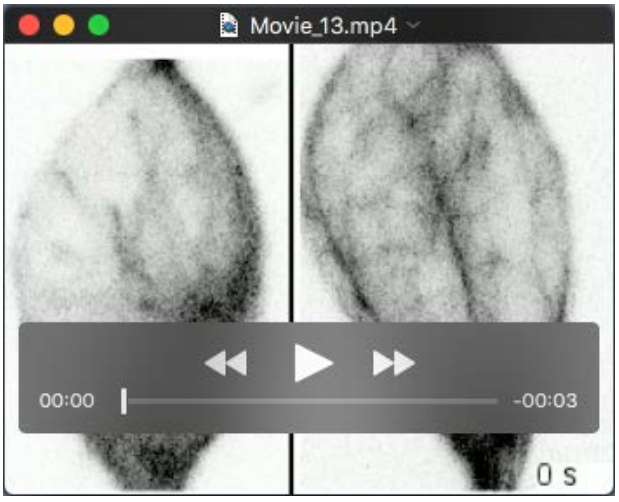

Movie 13. Growing microtubules around the nucleus in migrating CGCs. Time-lapse movies of CGCs expressing GFP-EB3 in vitro. Images were acquired every 3 sec for 150 sec.

Supplementary Materials and Methods

Antibodies

Antibodies used for immunostaining and western blotting were as follows: rabbit anti-Kif5B (1:500-1000, ab167429), anti-Lamin B1 (1:500, ab16048), rat anti-α-tubulin (1:1000, ab6160) purchased from Abcam; mouse anti-dynein intermediate chain (1:500-1000, MAB1618), HRP-conjugated anti-rabbit IgG (1:5000, AP182P) or anti-rat IgG (1:10000, AP183P) purchased from Millipore; goat anti-KLC1 (1:200, sc-13361), mouse anti-GFP (1:2000, sc-9996) purchased from Santa Cruz; mouse anti-acetylated tubulin (1:4000, T6793), anti-β-tubulin (1:1000, T4026) from Sigma; rabbit anti-GFP (1:2000, A11122), Alexa488-conjugated anti-mouse IgG (1:400, A21202; 1:400, A11029) or anti-rabbit IgG (1:400; A11034), Alexa568-conjugated anti-mouse IgG (1:400; A11004), anti-rabbit IgG (1:400, A11011) or anti-goat IgG (1:400, A11057), Alexa633-conjugated anti-mouse IgG (1:400, A21052) purchased from Molecular Probes; HRP-conjugated anti-rabbit IgG (1:10000, 170-6515) or anti-mouse IgG (1:10000, 170-6516) purchased from Bio-Rad.

Subcellular fractionation

Cerebella from P4 ICR mice were dissociated. Harvested CGCs were resuspended in a hypotonic buffer (10 mM HEPES pH7.9, 10 mM potassium chloride, 1.5 mM magnesium chloride, 1 mM EDTA, 1 mM DTT, and 1x protease inhibitor cocktail (Thermo Fisher)) on ice for 5 min, homogenized with a Dounce homogenizer, and centrifuged at 400 G for 5 min. The pellet was washed and saved as the nuclear fraction. The supernatant was further centrifuged at 10000 G for 10 min, and the resulting supernatant was saved as the cytosolic fraction. Proteins from each fraction were subjected to SDS-PAGE and western blotting.

Immunostaining of CGCs

Migrating CGCs in reaggregated cultures were fixed with 4% paraformaldehyde (PFA) in PBS and permeabilized with 0.3% Triton X-100 in PBS. For kinesin and dynein staining on the nuclear envelope, CGCs were treated with a hypotonic buffer (10 mM

HEPES pH7.9, 10 mM potassium chloride, 1.5 mM magnesium chloride, 1 mM EDTA, 1 mM DTT) on ice for 5 min before fixation. For tubulin staining with DCX-GFP overexpression, CGCs were fixed with methanol at -20 °C. Cells were washed with PBS, blocked with 2% skim milk, 0.1% Tween 20 in PBS, and subjected for immunostaining. The nuclei were stained with 4'-6-diamidino-2-phenylindole (DAPI)(Life technologies). Images were acquired with a laser-scanning confocal microscope FV1000 (Olympus) through a 100x oil-immersion objective (N.A. 1.4), or with LSM 880 with Airyscan (ZEISS) through a 100x oil-immersion objective (N.A. 1.46).

C2C12 cell culture and immunostaining

C2C12 cells were plated on poly-D-lysine coated coverslips and maintained at 37°C/5% CO_2 in RPMI with 10% fetal bovine serum and penicillin-streptomycin. Plasmid transfection were performed with Lipofectamine 2000. To induce myogenic differentiation, the media was changed to Dulbecco's Modified Eagle Medium with 2% horse serum. Differentiated C2C12 cells were fixed with 4% PFA in PBS and blocked with 2% skim milk, 0.3% Triton X-100 in PBS. Immunostaining was then performed with KLC1 and GFP antibodies, and stained with DAPI. Images were acquired with a laser-scanning confocal microscope FV1000 (Olympus) through a 100x oil-immersion objective (N.A. 1.4).

HEK293T cell culture and co-immunoprecipitation

HEK293T (RCB2202, RIKEN BRC) cells were maintained at 37°C/5% CO_2 in D-MEM with 10% fetal bovine serum and penicillin-streptomycin. GFP constructs transfection were performed with Lipofectamine 2000. Twenty hours post-transfection, cells were harvested in a lysis buffer (50 mM Tris-HCl pH7.4, 75 mM sodium chloride, 2.5 mM magnesium chloride, 1 mM EDTA, 1 mM DTT, 0.1% Triton-X100, and 1x protease inhibitor cocktail (Thermo Fisher)). Lysates were pre-cleared with Protein A/G PLUS Agarose beads (Santa Cruz) for 1 hr at 4°C. Mouse GFP antibody were added to the supernatant and incubated for 2.5 hr at 4°C. The beads were added to the sample and incubated for 1 hr at 4°C. The beads were washed with the lysis buffer for four times and subjected to SDS-PAGE and western blotting.